Chemical Physics **258** (2000) 73–96

Preprint of accepted version, references updated according to published version
File generated by M. Hoffmann on 11.07.2006

The Lowest Energy Frenkel and Charge-Transfer Excitons in Quasi-One-Dimensional Structures: Application to MePTCDI and PTCDA Crystals

M. Hoffmann,[1] K. Schmidt,[1] T. Fritz,[1] T. Hasche,[1] V.M. Agranovich,[2] and K. Leo[1]

[1]*Institut für Angewandte Photophysik, Technische Universität Dresden, 01062 Dresden, Germany*
[2]*Institute of Spectroscopy, Russian Academy of Sciences, Troitsk, Moscow obl., 142092 Russia*

We consider the exciton states in quasi-one-dimensional organic crystals with strong orbital overlap between neighboring molecules. In such crystals, the energy difference between the lowest Frenkel exciton and the nearest-neighbor charge-transfer excitons becomes small and their strong mixing determines the nature of the lowest energy states. We discuss these effects for crystalline MePTCDI (N-N′-dimethylperylene-3,4,9,10-dicarboximide) and PTCDA (3,4,9,10-perylenetetracarboxylic dianhydride). To model the exciton states we use a Hamiltonian which includes the mixing of Frenkel excitons with several vibronic levels and charge-transfer excitons. With appropriate fitting parameters, we demonstrate that this model can explain the main features of the low temperature absorption spectra. Polarized absorption spectra of MePTCDI show different polarization ratios for the various absorption peaks. This polarization behavior is discussed as a qualitative proof for the varying contribution of the charge-transfer excitons, which have a transition dipole direction different from that of the Frenkel excitons.

I. INTRODUCTION

It is well known that neutral electronic excitations, known as excitons, play a fundamental role in the determination of linear and nonlinear optical properties of dielectric solids [1]. This type of excitation corresponds to a bound state of an electron and a hole. It can be created by light or can appear as a result of relaxation processes of high energy excited states, e.g., states of free electrons and holes generated by electric pumping. Two models are usually employed to classify excitons - the small radius Frenkel exciton model, and the large radius Wannier-Mott exciton model.

The Wannier-Mott exciton model considers the coulombic interaction between two free particles and is based on the effective mass approximation for electrons and holes in the periodic crystal potential. Therefore, the internal structure of Wannier-Mott excitons can be represented by hydrogen-like functions. The mean electron-hole distance for this type of excitons should be large in comparison with the lattice constant. This condition can only be fulfilled if at least one of the charge carriers has a sufficiently small effective mass, i.e., if its bandwidth is large compared to the Coulomb attraction between electron and hole in the exciton. Such a situation is typical for inorganic semiconductors (Si, Ge, GaAs etc.) due to the large overlap of the atomic orbitals and the high dielectric constants.

On the other hand, the Frenkel exciton model considers a neutral excited state in which the electron and hole are placed on the same molecule. *Inter*molecular interactions give rise to a finite transfer integral for the transfer of the electronic excitation from one molecule to another. As a result, the Frenkel excitons are represented by one-particle excitation waves coherently propagating through the crystal. The Frenkel exciton model is applicable if the binding energy (i.e. the energy difference between a crystal with a free electron and hole with respect to the crystal with a Frenkel exciton) is large compared to both free carrier bandwidths.

The charge-transfer exciton (CTE) occupies an intermediate place in the classification of excitons based on their internal structure. A localized CTE configuration consists of a pair of charge carriers localized at different molecules. Such localization is supported in organic crystals, because, in contrast to inorganic semiconductors the binding energy of the lowest CTE is large compared to the valence and conduction bandwidth. The localization can also be stabilized due to a strong tendency of CTE to undergo self trapping [2]. In general, a CTE is a linear combination of such localized CTE configurations.

Charge-transfer excitons are currently considered as an important intermediate state in the creation of free carriers by light absorption [3]. Due to the large static dipole moment of the underlying localized CTE configurations (up to $10 - 25\,\mathrm{Debye}$ already for nearest-neighbor distances), CTE can cause large second order nonlinear polarizabilities $\chi^{(2)}$ (see, for example, [4]) and strong electro-absorption signals [5, 6].

As soon as the energetic difference between a CTE configuration and a Frenkel exciton becomes small, both excitons can interact and form new mixed states. These mixed Frenkel-charge-transfer excitons show properties of both types of contributing states: The Frenkel exciton provides a large oscillator strength, whereas the CTE causes a high sensitivity to external electric fields. The first model for the mixing of Frenkel and CT excitons was presented by Merrifield [7]. As long as only CTE with small electron-hole separation are included, such a model has still to be considered as a small radius exciton model.

For organic polyacene crystals, this concept was successfully used to describe the low energy excitons observed in electro-absorption experiments [8]. In anthracene, e.g., the

electronically and vibrationally lowest excited state is still an almost pure Frenkel exciton, whereas mixing between Frenkel and CT excitons occurs in the region of its vibronic replicas. Furthermore, the CTE binding energy in anthracene is much larger than the carrier bandwidth so that the restriction to Frenkel and nearest-neighbor CT excitons is self-consistently justified. In this way, many qualitative and quantitative features of the low energy excited states in crystals of the anthracene type are already well understood in terms of such a small radius exciton model.

Nevertheless, there is an increasing interest in such exciton models, since a permanently rising number of new organic crystals become important for thin film device applications. From this point of view, special attention is deserved by so-called quasi-one-dimensional molecular crystals, in which the distance between molecules in one direction is much smaller than in the others. Usually, such structures are formed by planar aromatic molecules which arrange in one-dimensional face-to-face stacks with strong *inter*molecular overlap of the π-orbitals. A number of perylene derivatives are prominent examples for 1D crystals. They are not only interesting for photo-electric device applications like solar cells [9] or xerography [10] but they are extensively studied due to their capability of ordered growth on several substrates (reviewed in [11]).

In this paper, we will study crystals of MePTCDI (N-N′-dimethylperylene-3,4,9,10-dicarboximide) and PTCDA (3,4,9,10-perylenetetracarboxylic dianhydride). The distance between the molecular planes within the one-dimensional stacks (3.40 Å for MePTCDI [12] and 3.37 Å for PTCDA, derived from [13–16]) is small in comparison with other lattice constants and also small in comparison with the size of the molecules. This causes strong interactions of the π-electron systems within the stacks, but a very weak interaction in the other directions. Due to these strong interactions in the stack it is not obvious which exciton models are best suited.

We can expect that in such crystals the qualitative difference between Frenkel and CT excitations becomes smaller, their energies approach each other and their strong mixing determines the nature of the lowest energy states. For a qualitative illustration of this physical picture, we present in Fig. 1 the results of quantum chemical calculations for the simplest model system: a dimer of two ethylene molecules. The position of the second molecule with respect to the first is given by a translation of distance r along the symmetry axis perpendicular to the molecular plane (see inset in Fig. 1). In Fig. 1, the energy of the four lowest excited states is given as a function of the distance r.

At large distances r, the situation represents the conditions in anthracene-like crystals: The lowest states of the dimer are two Frenkel states and there are two CT states well separated at higher energies. As could be expected, for large distances the energy of the CT states as a function of r follows the relation: $E = I - A - e^2/r$, where I is the ionization energy and A is the electron affinity of the monomer. It is clear that for such large distances the *inter*molecular overlap between the π-orbitals is small and therefore, the transition dipole moment from the ground to the CT state should also be small. With

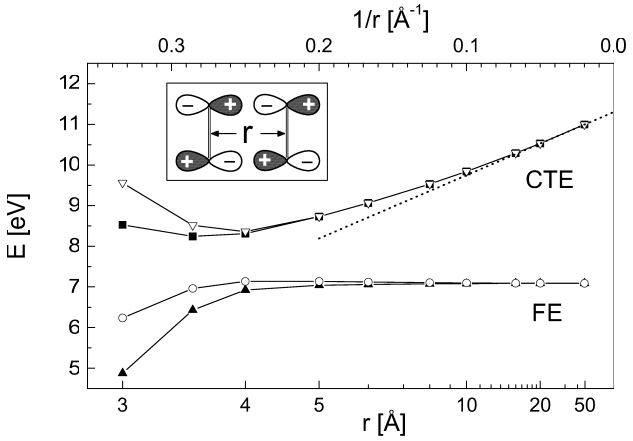

FIG. 1: Calculated energy of the four lowest excited states in a model dimer of two ethylene molecules (geometry see inset). r is the distance between the molecular planes. For $r \geq 10$ Å, there are two degenerate Frenkel excitons (corresponding to molecular excitations) and two degenerate charge-transfer excitons. Calculations with ZINDO/S module of HyperChem.

decreasing the distance r, the energy of the CT states will decrease and they will inevitably become resonant with the Frenkel states. In combination with increasing orbital overlap and increasing charge-transfer integrals, this leads to a repulsion of levels and strong mixing of all states with the same symmetry. Furthermore, even the pure CT states can attain a considerable transition dipole moment due the finite orbital overlap. In the model calculation, the strong mixing occurs at distances below 3.5 Å, which is a typical distance between molecular planes in quasi-1D crystals.

In the present paper, we assume that such a situation occurs in MePTCDI and similar crystals. We discuss this phenomenon in the framework of a one-dimensional model Hamiltonian which includes Frenkel and nearest-neighbor CT excitons. This model is capable of describing the main features of the absorption spectrum within the conditions necessary for a small radius exciton model. In extension to the model for PTCDA-dimers developed by Hennessy et al. [17], we consider an infinite chain and explicitly analyze the intrinsic transition dipole moment of the CTE. In connection with polarized absorption spectra of MePTCDI, this analysis is used as a direct qualitative proof for the contribution of CT excitons. This analysis is the extension of our preliminary results for the Frenkel-CT-mixing in MePTCDI presented in [18].

The paper is organized as follows: In section 2, we will first review the available information about excitons in MePTCDI and related crystals. Then, we will qualitatively describe the features of our approach. A self-contained formulation of our model is provided in section 3. In section 4, the absorption experiments and the processing of the raw spectra are described. The detailed analysis of these experimental data by means of the model from section 3 is presented in the fifth section. Our analysis is supported by preliminary quantum chemical calculations. However, only the direction of the CTE transition dipole moment is actually employed in our model. Therefore,

we give only a schematic description of these calculations in the Appendix.

II. THE QUASI-ONE-DIMENSIONAL CRYSTALS MEPTCDI AND PTCDA

In the following, we will consider quasi-one-dimensional crystals of the perylene derivatives MePTCDI and PTCDA. During the last years, intensive investigations of UV-VIS-absorption (e.g. [12, 19]), electro-absorption [20], IR and Raman spectra [21, 22], photoluminescence [23–26], photoconductivity [10, 27] and photo-emission [28] were performed in order to establish the nature of the lowest energy states in such crystals.

The excited states of the isolated molecules are well understood. For similar compounds they were studied by quantum chemical methods (INDO level) by Adachi et al. [29]. In our own calculations (ZINDO/S, see Appendix) we found results very similar to Adachi's for MePTCDI and PTCDA. In Fig. 2a we show the absorption spectrum of MePTCDI dissolved in chloroform. The solution spectrum of PTCDA (in DMSO) looks almost identical. The three strong absorption bands in the visible range belong to the lowest π-π^*-transition of the extended π-electron system. Therefore, this lowest singlet state S_1 is only weakly affected by chemical substitutions. The S_0-S_1 transition is polarized along the long molecular axis, and from the absolute absorption cross section we estimate its total electronic transition dipole to be $p_1 = 6.8\,\mathrm{Debye}$ (see section 4). The next highest dipole allowed singlet state S_2 has a much smaller transition dipole directed along the short axis in the molecular plane (M-axis). It is associated with the very weak structure in the solution spectra (Fig. 2) at $3.4\,\mathrm{eV}$, which has an estimated transition dipole of less than $1.8\,\mathrm{Debye}$.

The electronic S_0-S_1 transition strongly couples to C-C and C=C stretching modes of the carbon backbone, which leads to the vibronic progression seen in Fig. 2a [17, 29]. From resonant Raman scattering data [22] it follows that in fact there are several energetically close vibrational modes with large exciton-phonon-coupling constants. In the UV-VIS-spectra they are not resolved and can be treated as one effective mode with an effective coupling constant as done in [17].

In the crystalline phase, the excited states of the monomer are strongly influenced by *inter*molecular interactions, which leads to dramatic changes in the absorption spectra (MePTCDI in Fig. 2b and PTCDA in Fig. 2c). Although very similar in their monomer spectra, MePTCDI and PTCDA differ considerably in their crystal spectra. This difference is caused by the steric effects of the substituents which results in a different geometrical arrangement of the molecules with respect to each other. Such effects, known as crystallochromy, were studied empirically for a large number of perylene derivatives (e.g. [12, 30] and references therein).

The first microscopic model for trends in the crystal spectra of such perylenes was proposed by Kazmaier and Hoffmann [31]. They studied the one-particle band structures that arise from the overlap of the molecular HOMO's and LUMO's in

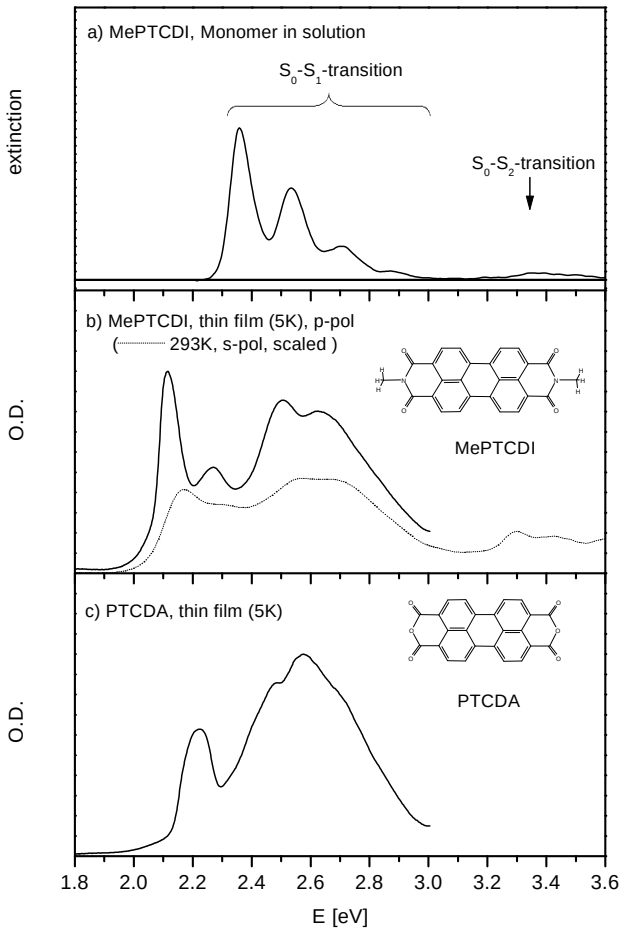

FIG. 2: Comparison of monomer and crystal spectra. a) Molar extinction coefficient of isolated MePTCDI molecules ($0.5\,\mu\mathrm{M}$ solution in chloroform, room temperature). b) Optical density spectrum of poly-crystalline MePTCDI (1) for highly oriented domain in thin film at $5\,\mathrm{K}$, p-polarized and (2) for a larger area of the thin film at room temperature, s-polarized, to show the region of the S_0-S_2-transition. c) Optical density spectrum of crystalline PTCDA (thin film at $5\,\mathrm{K}$, spectrum is independent of polarization)

the crystal at extended Hückel level. They clearly described how the one-particle band structure depends in a very subtle way on the geometric arrangement of the molecules. However, this model in itself does not yet explain the observed peak structure of the optical spectra. In our approach, we assume that the lowest states seen in the optical spectra are dominated by small radius excitons, which are energetically well below and qualitatively very different from one-particle band-to-band excitations.

First attempts to explain the structure of the PTCDA absorption spectrum were made in the framework of three-dimensional Wannier-Mott exciton models for the lowest energy absorption peak at 2.2 eV [32, 33]. Later, this peak was assigned to a CT exciton in order to explain electro-absorption experiments [20]. In this line of studies Bulovic et al. gave an interpretation of the PTCDA crystal spectrum in terms of Frenkel and localized CT excitons [19]. Still, no interactions within the exciton manifold were considered. In such a model,

especially the high absorption cross section of the CT exciton remains implausible.

The description of the PTCDA spectrum in the framework of a dimer model with interaction of Frenkel and CT excitons was presented by Hennessy, Soos, Pascal and Girlando in [17]. In their model, the lowest excited states are described as strongly mixed states that contain the lowest Frenkel exciton and the lowest CT exciton, each with its vibronic replicas. Due to the mixing, the oscillator strength of the Frenkel exciton is distributed to all states, and the spectra are explained without consideration of an intrinsic CTE transition dipole. However, this model is not able to describe a variation of the polarization ratio for different absorption peaks, which we observe in polarized absorption spectra of MePTCDI.

In our paper we present a model which also includes interactions between Frenkel and CT excitons. Instead of a Holstein model as in [17], we consider the case of strong exciton-phonon coupling, which is a very good approximation (see below) and allows an exact solution for the infinite chain. Furthermore, we use a simplified picture for the vibronic states. Our main intention is to discuss a new feature: If in quasi-1D crystals the *inter*molecular π-orbital-overlap is large enough to cause strong mixing between Frenkel and CT excitons, then this overlap can also be sufficient to produce an observable transition dipole for CT excitons. Only the inclusion of this intrinsic charge-transfer transition dipole can explain the experimentally observed polarization behavior.

The low temperature absorption spectrum of MePTCDI crystals is roughly characterized by four peaks (cf. Fig. 2b). Since the lowest energy monomer absorption is dominated by only three peaks, it can be well described by the lowest energy electronic transition with three molecular vibronic levels. These three molecular levels become three mixed exciton bands if we take into account the mixing of molecular configurations arising due to *inter*molecular resonance interaction. However, such a Frenkel exciton model can not explain the four significant peaks in the spectrum of the crystal. To achieve that, we also consider mixing with nearest-neighbor charge-transfer configurations.

We will show below that the existence of a low energy CTE and its mixing with Frenkel exciton states gives a natural possibility to explain not only the appearance of an additional peak in the absorption spectra but also to explain the observed polarization dependencies. Since MePTCDI and PTCDA are crystals with two molecules per unit cell, the transition dipole of an individual stack can not be directly probed anymore. In this case, only the polarization ratio R is the externally observable manifestation of the polarization direction of the individual 1D excitons (cf. section 3). In our polarized absorption spectra of MePTCDI, we see different ratios R for the various exciton states (cf. Fig. 4). This means that the exciton states in the one-dimensional stacks must have a varying polarization, which deviates from the direction of the long molecular axis.

The existence of such a deviation is in agreement with symmetry considerations: Indeed, in both MePTCDI and PTCDA crystals, the individual stacks have a stacking direction, which is not perpendicular to the molecular plane. In a projection on the molecular planes, two neighboring molecules are shifted with respected to each other in both the directions of the long and the median (M-) molecular axis. Due to this shift, an individual stack belongs to a class of crystals with the symmetry site group $\mathbf{C}_i$. That means that the transition dipole moment from the ground state to the dipole allowed excited states can have three nonvanishing components P_x, P_y, P_z. If we take the x-axis along the long molecular axis, the lowest excited molecular state has its transition dipole only in the x direction. The reason for the appearance of nonzero components P_y, P_z in the stack can only be the mixing with other *intra-* or *inter*molecular configurations having a different polarization. For example, this might be the second excited molecular state, which is polarized along the M-axis. However, in section 5 we will estimate that this state does by far not sufficiently mix to explain the experimentally observed polarization ratios. We therefore consider the mixing with the lowest energy CT excitons as the reason for the appearance of new transition dipole components.

The direction of the CT transition dipole cannot be estimated from symmetry considerations. In the Appendix, we will show that the CT transition dipole lies approximately in the molecular plane and has a large component parallel to the molecular M-axis. Thus, a varying mixing with this CT state can explain the varying polarization ratio, which would otherwise be an implausible phenomenon even on a qualitative level.

III. MODEL HAMILTONIAN AND MIXING OF FRENKEL AND CHARGE-TRANSFER STATES

For the description of the excited states in a one-dimensional molecular crystal with one molecule per unit cell we use the following Hamiltonian:

$$\begin{aligned}
\mathcal{H} &= \mathcal{H}^{\mathrm{F}} + \mathcal{H}^{\mathrm{FF}} + \mathcal{H}^{\mathrm{C}} + \mathcal{H}^{\mathrm{FC}} \\
\mathcal{H}^{\mathrm{F}} &= \sum_{n\nu} \Delta_{\mathrm{F}}^{\nu} \mathcal{B}_{n\nu}^{\dagger} \mathcal{B}_{n\nu} \\
\mathcal{H}^{\mathrm{FF}} &= {\sum_{\substack{n\nu \\ m\mu}}}' M_{nm}^{\nu\mu} \mathcal{B}_{n\nu}^{\dagger} \mathcal{B}_{m\mu} \\
\mathcal{H}^{\mathrm{C}} &= \sum_{n\sigma} \Delta_{\mathrm{CT}} \mathcal{C}_{n\sigma}^{\dagger} \mathcal{C}_{n\sigma} \\
\mathcal{H}^{\mathrm{FC}} &= \sum_{n\nu} \big\{ \epsilon_{\mathrm{e}}^{\nu} (\mathcal{B}_{n\nu}^{\dagger} \mathcal{C}_{n,+1} + \mathcal{B}_{n\nu}^{\dagger} \mathcal{C}_{n,-1}) \\
&\quad + \epsilon_{\mathrm{h}}^{\nu} (\mathcal{B}_{n\nu}^{\dagger} \mathcal{C}_{n+1,-1} + \mathcal{B}_{n\nu}^{\dagger} \mathcal{C}_{n-1,+1}) \big\} + \mathrm{h.c.} \quad (1)
\end{aligned}$$

Here the operator $\mathcal{B}_{n\nu}^{\dagger}$ ($\mathcal{B}_{n\nu}$) describes the creation (annihilation) of a neutral molecular excitation (Frenkel exciton) at lattice site n. Only one electronically excited molecular state is considered, and the index ν specifies the excited vibrational level ($\nu = 0, 1, \ldots, \nu_{\max}$). Then, $\Delta_{\mathrm{F}}^{\nu}$ is the on-site energy of a Frenkel exciton and $M_{nm}^{\nu\mu}$ the hopping integral for excitation transfer from level ν at site n to level μ at site m. In the summation in $\mathcal{H}^{\mathrm{FF}}$ the terms for $n = m$ are omitted.

The Hamiltonian $\mathcal{H}^{\rm F} + \mathcal{H}^{\rm FF}$ can be used to describe the mixing of molecular configurations for Frenkel excitons with several excited states in Heitler-London approximation. The mixing of molecular configurations in the theory of Frenkel excitons was considered by Craig [34, 35]. Craig demonstrated that the intensities of the weak lowest energy transitions in some organic crystals can not be explained by an electronic two-level model for the molecules constituting the crystal. Rather, it is necessary to take into account the higher excited molecular states and the mixing of molecular configurations arising due to the *inter*molecular interaction. In this theory, the *inter*molecular interaction was considered to be small in comparison with the separation between the excited state levels. A more general theory of Frenkel excitons in molecular crystals developed by Agranovich [36, 37] gave the possibility to consider also the mixing of molecular excited states with close energies. In $\mathcal{H}^{\rm FF}$ from (1) we use this formulation (reviewed in e.g. [38, 39]) and consider explicitly all interactions between the various molecular configurations.

Since we use only the operators $\mathcal{B}^\dagger_{n\nu}$ in (1) to describe the electronic *and* vibrational state of molecule n, we neglect the configurations in which the exciton and an (*intra*molecular) optical phonon are located on different molecules. This approximation corresponds to the limit of strong exciton-phonon coupling. With an accuracy of ≈5% it gives the same exciton bandwidth for PTCDA as obtained in [40], where all possible exciton - optical phonon configurations were taken into account. Such a result could be qualitatively expected because in PTCDA (and similarly in MePTCDI) the exciton-phonon coupling constant g=0.84 (as used in [40]) is rather large.

In the present paper, we also include the nearest-neighbor charge transfer excitons, in addition to the Frenkel excitons. A localized CT exciton with the hole at lattice site n and the electron at lattice site $n+\sigma$ ($\sigma = -1, +1$) is created (annihilated) by the operator $\mathcal{C}^\dagger_{n\sigma}$ ($\mathcal{C}_{n\sigma}$). For simplicity, only the vibrational ground state is considered for the CT excitons with $\Delta_{\rm CT}$ as their on-site energy. Hopping of CT states will not be considered.

The mixing between Frenkel and CT excitons is expressed in the last part $\mathcal{H}^{\rm FC}$ of the Hamiltonian. Here, the transformation of a CT state into any Frenkel state at the lattice site of either hole or electron is allowed. The relevant transfer integrals $\epsilon^\nu_{\rm e}$ ($\epsilon^\nu_{\rm h}$) can be visualized as transfer of an electron (hole) from the excited molecule n to its nearest-neighbor. With this formulation of the Hamiltonian $\mathcal{H}^{\rm FC}$, the CT excitons are mathematically treated just like another molecular excitation.

In order to diagonalize the Hamiltonian, we first transform all operators into their momentum space representation:

$$\mathcal{B}_{k\nu} := \frac{1}{\sqrt{N}} \sum_n {\rm e}^{-{\rm i}kn} \mathcal{B}_{n\nu} \tag{2}$$

$$\mathcal{C}_{k\sigma} := \frac{1}{\sqrt{N}} \sum_n {\rm e}^{-{\rm i}kn} \mathcal{C}_{n\sigma} \tag{3}$$

Then the Hamiltonian takes the form:

$$\begin{aligned}
\mathcal{H} &= \sum_k \left(\mathcal{H}^{\rm F}_k + \mathcal{H}^{\rm FF}_k + \mathcal{H}^{\rm C}_k + \mathcal{H}^{\rm FC}_k \right) \\
\mathcal{H}^{\rm F}_k &= \sum_\nu \Delta^\nu_{\rm F} \mathcal{B}^\dagger_{k\nu} \mathcal{B}_{k\nu} \\
\mathcal{H}^{\rm FF}_k &= \sum_{\nu\mu} L^{\nu\mu}_k \mathcal{B}^\dagger_{k\nu} \mathcal{B}_{k\mu} \\
\mathcal{H}^{\rm C}_k &= \sum_\sigma \Delta_{\rm CT} \mathcal{C}^\dagger_{k\sigma} \mathcal{C}_{k\sigma} \\
\mathcal{H}^{\rm FC}_k &= \sum_\nu \mathcal{B}^\dagger_{k\nu} \left\{ (\epsilon^\nu_{\rm e} + \epsilon^\nu_{\rm h} {\rm e}^{{\rm i}k}) \mathcal{C}_{k,+1} \right. \\
&\quad \left. + (\epsilon^\nu_{\rm e} + \epsilon^\nu_{\rm h} {\rm e}^{-{\rm i}k}) \mathcal{C}_{k,-1} \right\} + {\rm h.c.}
\end{aligned} \tag{4}$$

Here, the symbol $L^{\nu\mu}_k$ is used to abbreviate the lattice sum

$$L^{\nu\mu}_k := {\sum_m}' {\rm e}^{{\rm i}km} M^{\nu\mu}_{0m} \; . \tag{5}$$

The Hamiltonian (4) is already diagonal with respect to k. It still contains mixed terms of the $\nu = 0, \ldots, \nu_{\rm max}$ operators for the Frenkel excitons and the two operators for CT excitons. These are altogether $\nu_{\rm max}+3$ molecular configurations, which would yield $\nu_{\rm max}+3$ mixed exciton bands.

With several simplifying assumptions we now reduce the number of parameters in the Hamiltonian, which also allows the separation of one non-mixing exciton band. The parameters are given by the transition matrix elements with the considered states. Using product wave functions in Born-Oppenheimer approximation, we can write for the ground state

$$|0\rangle = |\prod_n \varphi^0_n \chi^{00}_n \rangle^{(-)} \tag{6}$$

and for the Frenkel excitons

$$\mathcal{B}^\dagger_{n\nu}|0\rangle = |\varphi^1_n \chi^{1\nu}_n \prod_{n' \neq n} \varphi^0_{n'} \chi^{00}_{n'} \rangle^{(-)} \; . \tag{7}$$

Here φ^0_n and φ^1_n denote the electronic part of the wave function of molecule n in the ground and first electronically excited state. $\chi^{\mu\nu}_n$ is the vibrational wave function of molecule n in its μth electronic and νth vibrational state. The upper index $^{(-)}$ at the Dirac bracket indicates that the product wave function is antisymmetrized with respect to all electrons. The CT states are represented by:

$$\mathcal{C}^\dagger_{n,+1}|0\rangle = |\varphi^+_n \chi^{+0}_n \varphi^-_{n+1} \chi^{-0}_{n+1} \prod_{\substack{n' \neq n \\ n' \neq n+1}} \varphi^0_{n'} \chi^{00}_{n'} \rangle^{(-)} \; , \tag{8}$$

$$\mathcal{C}^\dagger_{n,-1}|0\rangle = |\varphi^-_{n-1} \chi^{-0}_{n-1} \varphi^+_n \chi^{+0}_n \prod_{\substack{n' \neq n \\ n' \neq n-1}} \varphi^0_{n'} \chi^{00}_{n'} \rangle^{(-)} \; , \tag{9}$$

where $\varphi^\pm_n$ and $\chi^\pm_n$ refer to the ionized molecules.

Using these representations, the Frenkel exciton transfer integral can be split into an electronic and a vibronic part:

$$\begin{aligned}
M^{\nu\mu}_{nm} &= \langle \mathcal{B}^\dagger_{n\nu} 0 | \mathcal{H} | \mathcal{B}^\dagger_{m\mu} 0 \rangle \\
&= M_{nm} s_\nu s_\mu
\end{aligned} \tag{10}$$

The vibronic overlap factors

$$s_\nu = \langle \chi^{1\nu}_n | \chi^{00}_n \rangle \tag{11}$$

defined here are directly related to the Franck-Condon factors $F_{0\nu} = |\langle\chi^{1\nu}|\chi^{00}\rangle|^2$. Since the Frenkel exciton transfer integrals M_{nm} in dipole approximation are decreasing with distance by $(n-m)^{-3}$, we can neglect all but nearest-neighbor transfer in the one-dimensional case:

$$M_{nm} = \delta_{n\pm1,m} M \tag{12}$$

with M being the nearest-neighbor exciton transfer integral. With this approximation, $L_k^{\nu\mu}$ from (5) is reduced to

$$L_k^{\nu\mu} = 2M s_\nu s_\mu \cos k \; . \tag{13}$$

The vibrational overlap factors for the Frenkel states can be easily derived from the absorption spectrum of the molecule in solution. Since the coupling to *intra*molecular vibrations is in our case strong compared to *inter*molecular phonon coupling, the overlap factors from isolated molecules can be used for the crystalline phase as well.

For CT excitons the situation is different. There is no direct access to the vibrational overlap factors connected with χ_n^{+0} and χ_n^{-0}. We therefore make the strongly simplifying assumption that

$$\chi_n^{+0} = \chi_n^{-0} = \chi_n^{00} \; , \tag{14}$$

which corresponds to neglecting the vibrational relaxation of the ionized molecules. The relaxation energy of an ion is expected to be smaller than that of the excited singlet state since only in one orbital the occupation is changed. Quantum chemical calculations for PTCDA [41] give indeed smaller relaxation energies of 72 meV (cation) and 127 meV (anion) compared to 323 meV for the excited singlet. A similar trend is confirmed for the relaxation energy of the anion in [42]. Although smaller than for the singlet, such relaxation energies would still have a considerable influence. In this paper, we nevertheless prefer to use the approximation (14) since it provides a conceptually simple qualitative model with a minimum set of parameters and states.

Then we obtain

$$\begin{aligned}
\epsilon_{\rm e}^\nu &= \langle \mathcal{B}_{n\nu}^\dagger 0|\mathcal{H}|\mathcal{C}_{n,+1}^\dagger 0\rangle \\
&= \underbrace{{}^{(-)}\langle\varphi_n^1 \prod_{n'\neq n}\varphi_{n'}^0|\mathcal{H}|\varphi_n^+\varphi_{n+1}^- \prod_{\substack{n'\neq n\\ n'\neq n+1}}\varphi_{n'}^0\rangle^{(-)}}_{\epsilon_{\rm e}} \underbrace{\langle\chi_n^{1\nu}|\chi_n^{00}\rangle}_{s_\nu} \\
&= \epsilon_{\rm e} s_\nu
\end{aligned} \tag{15}$$

$$\begin{aligned}
\epsilon_{\rm h}^\nu &= \langle \mathcal{B}_{n\nu}^\dagger 0|\mathcal{H}|\mathcal{C}_{n+1,-1}^\dagger 0\rangle \\
&= \underbrace{{}^{(-)}\langle\varphi_n^1 \prod_{n'\neq n}\varphi_{n'}^0|\mathcal{H}|\varphi_n^-\varphi_{n+1}^+ \prod_{\substack{n'\neq n\\ n'\neq n+1}}\varphi_{n'}^0\rangle^{(-)}}_{\epsilon_{\rm h}} \underbrace{\langle\chi_n^{1\nu}|\chi_n^{00}\rangle}_{s_\nu} \\
&= \epsilon_{\rm h} s_\nu
\end{aligned} \tag{16}$$

With these simplifications, the Hamiltonian for the Frenkel-CT-mixing becomes:

$$\begin{aligned}
\mathcal{H}_k^{\rm FC} \;=\; & \sum_\nu s_\nu \mathcal{B}_{k\nu}^\dagger \left\{(\epsilon_{\rm e}+\epsilon_{\rm h}{\rm e}^{{\rm i}k})\mathcal{C}_{k,+1}\right. \\
& \left. +(\epsilon_{\rm e}+\epsilon_{\rm h}{\rm e}^{-{\rm i}k})\mathcal{C}_{k,-1}\right\} + {\rm h.c.}
\end{aligned} \tag{17}$$

We now introduce two new operators with even and odd symmetry with respect to change of the direction of the charge transfer:

$$\begin{aligned}
\tilde{\mathcal{C}}_{k{\rm g}} \;:=\; & \frac{1}{\sqrt{2}\epsilon_k}\cdot\left\{(\epsilon_{\rm e}+\epsilon_{\rm h}{\rm e}^{{\rm i}k})\mathcal{C}_{k,+1}\right. \\
& \left. +(\epsilon_{\rm e}+\epsilon_{\rm h}{\rm e}^{-{\rm i}k})\mathcal{C}_{k,-1}\right\}
\end{aligned} \tag{18}$$

$$\begin{aligned}
\tilde{\mathcal{C}}_{k{\rm u}} \;:=\; & \frac{1}{\sqrt{2}\epsilon_k}\cdot\left\{(\epsilon_{\rm e}+\epsilon_{\rm h}{\rm e}^{{\rm i}k})\mathcal{C}_{k,+1}\right. \\
& \left. -(\epsilon_{\rm e}+\epsilon_{\rm h}{\rm e}^{-{\rm i}k})\mathcal{C}_{k,-1}\right\} \; ,
\end{aligned} \tag{19}$$

where

$$\epsilon_k := \sqrt{\epsilon_+^2\cos^2\frac{k}{2} + \epsilon_-^2\sin^2\frac{k}{2}} \tag{20}$$

with

$$\epsilon_\pm := \epsilon_{\rm e} \pm \epsilon_{\rm h} \; . \tag{21}$$

The Hamiltonian for the CT states then simplifies to:

$$\mathcal{H}_k^{\rm C} \;=\; \Delta_{\rm CT}\left\{\tilde{\mathcal{C}}_{k{\rm g}}^\dagger\tilde{\mathcal{C}}_{k{\rm g}} + \tilde{\mathcal{C}}_{k{\rm u}}^\dagger\tilde{\mathcal{C}}_{k{\rm u}}\right\} \tag{22}$$

$$\mathcal{H}_k^{\rm FC} \;=\; \sum_\nu \sqrt{2}\epsilon_k s_\nu\cdot\mathcal{B}_{k\nu}^\dagger\tilde{\mathcal{C}}_{k{\rm g}} \;+\; {\rm h.c.} \tag{23}$$

The odd operator $\tilde{\mathcal{C}}_{k{\rm u}}$ does not mix with the Frenkel operators anymore, which reduces the number of mixed exciton bands by one. The remaining even part $\mathcal{H}_k^{\rm g}$ of the Hamiltonian can be formally diagonalized by transformation to new operators $\xi_{k\beta}$

$$\xi_{k\beta} := \sum_{\nu=0}^{\nu_{\max}}\left\{u_{\nu\beta}^*(k)\mathcal{B}_{k\nu}\right\} + c_\beta^*(k)\tilde{\mathcal{C}}_{k{\rm g}} \tag{24}$$

where the transformation matrix $(u_{\nu\beta}, c_\beta)$ is the solution of the Eigenvalue problem for the matrix $H_{\alpha\beta}$ of the coefficients in the Hamiltonian:

$$H_{\alpha\beta} = \left(\begin{array}{c|c} \left(\begin{array}{c}\vdots\\ \cdots\;\; \delta_{\nu\mu}\Delta_{\rm F}^\nu + 2Ms_\nu s_\mu\cos k \;\; \cdots\\ \vdots\end{array}\right)_{\nu\mu} & \left(\begin{array}{c}\vdots\\ \sqrt{2}\epsilon_k s_\nu\\ \vdots\end{array}\right)_\nu \\ \hline \left(\cdots\;\; \sqrt{2}\epsilon_k s_\mu \;\; \cdots\right)_\mu & \Delta_{\rm CT}\end{array}\right) \tag{25}$$

The diagonalization of this matrix was always carried out numerically. Since $H_{\alpha\beta}$ is real and symmetric, the transformation matrix is also real, and we omit the notation for the complex conjugate from now on.

With the knowledge of the excited states we can also calculate the transition dipole moments for optical excitation. From (20) it follows for $k = 0$ that $\mathcal{H}_{k=0}^{\rm FC}$ is only determined by $\epsilon_{k=0} = |\epsilon_+|$. If $\vec{\mathcal{P}}$ is the total transition dipole operator, the

transition dipole moment for the state $\xi^\dagger_{k=0,\beta}|0\rangle$ can be expressed as a sum of Frenkel and CT transition dipoles:

$$\begin{aligned}\vec{P}^\beta &= \langle \xi^\dagger_{k=0,\beta} 0|\vec{\mathcal{P}}|0\rangle \\ &= \underbrace{\sum_{\nu=0}^{\nu_{\max}} u_{\nu\beta(k=0)} \cdot \langle \mathcal{B}^\dagger_{0\nu} 0|\vec{\mathcal{P}}|0\rangle}_{\text{FE}} + \underbrace{c_{\beta(k=0)} \cdot \langle \tilde{\mathcal{C}}^\dagger_{0g} 0|\vec{\mathcal{P}}|0\rangle}_{\text{CT}} \\ &= \vec{P}^\beta_{\text{FE}} + \vec{P}^\beta_{\text{CT}} \end{aligned} \quad (26)$$

These transition dipoles can be related to molecular properties as follows: For the Frenkel exciton part we obtain with (2) and (7):

$$\begin{aligned}\vec{P}^\beta_{\text{FE}} = & \sum_{\nu=0}^{\nu_{\max}} u_{\nu\beta(k=0)}\, s_\nu \cdot \frac{1}{\sqrt{N}} \\ & \times \sum_n {}^{(-)}\langle \varphi^1_n \prod_{n'\neq n} \varphi^0_{n'} |\vec{\mathcal{P}}| \prod_{n''} \varphi^0_{n''} \rangle^{(-)} \end{aligned} \quad (27)$$

If *inter*molecular exchange effects are neglected in this expression, $\vec{\mathcal{P}}$ can be split into a sum of molecular transition dipole operators $\vec{\mathcal{P}}_n$ with $\vec{p}_{\text{ME}} = \langle \varphi^1_n |\vec{\mathcal{P}}_n| \varphi^0_n\rangle$ being the transition dipole moment of a molecular excitation:

$$\vec{P}^\beta_{\text{FE}} = \sqrt{N}\vec{p}_{\text{ME}} \cdot \sum_{\nu=0}^{\nu_{\max}} u_{\nu\beta(k=0)}\, s_\nu$$

Using the abbreviation

$$U_\beta(k) := \sum_{\nu=0}^{\nu_{\max}} u_{\nu\beta}(k)\, s_\nu \,, \quad (28)$$

the Frenkel part of the transition dipole can be written as:

$$\vec{P}^\beta_{\text{FE}} = \sqrt{N}\vec{p}_{\text{ME}} \cdot U_{\beta(k=0)} \quad (29)$$

In the same way, we obtain from (8), (9) and with (14):

$$\begin{aligned}\vec{P}^\beta_{\text{CT}} &= c_{\beta(k=0)} \frac{1}{\sqrt{N}} \sum_n \\ &\times {}^{(-)}\langle \underbrace{\frac{\varphi^+_n \varphi^-_{n+1} + \varphi^-_n \varphi^+_{n+1}}{\sqrt{2}}}_{|\text{CT}^{\text{g}}_n\rangle} \prod_{\substack{n'\neq n \\ n'\neq n+1}} \varphi^0_{n'} |\vec{\mathcal{P}}| \prod_{n''} \varphi^0_{n''} \rangle^{(-)} \end{aligned} \quad (30)$$

Here, we can separate an even CT state for a dimer $|\text{CT}^{\text{g}}_n\rangle = |1/\sqrt{2}(\varphi^+_n\varphi^-_{n+1} + \varphi^-_n\varphi^+_{n+1})\rangle^{(-)}$ with a transition dipole $\vec{p}_{\text{CT}}$. If we again neglect exchange of electrons between the CT dimer and the other molecules in the ground state, we obtain:

$$\vec{P}^\beta_{\text{CT}} = \sqrt{N}\vec{p}_{\text{CT}} \cdot c_{\beta(k=0)} \quad (31)$$

The state $|\text{CT}^{\text{g}}_n\rangle$ corresponds to the symmetric CT state $|\text{CT}_+\rangle$ of an isolated dimer, which is analyzed in the Appendix: We show there that $\vec{p}_{\text{CT}}$ can have a considerable value and a different direction compared to $\vec{p}_{\text{ME}}$. Below, we express the total transition dipole $\vec{P}^\beta$ in (26) by means of the unit vectors $\vec{t}_{\text{ME}} := \vec{p}_{\text{ME}}/p_{\text{ME}}$ and $\vec{t}_{\text{CT}} := \vec{p}_{\text{CT}}/p_{\text{CT}}$. Using the relative CT transition dipole $p^{\text{rel}}_{\text{CT}} := p_{\text{CT}}/p_{\text{ME}}$, we obtain from (29) and (31):

$$\vec{P}^\beta = \sqrt{N}p_{\text{ME}} \cdot \Big(\underbrace{U_{\beta(k=0)}\vec{t}_{\text{ME}}}_{\text{FE}} + \underbrace{p^{\text{rel}}_{\text{CT}} c_{\beta(k=0)}\vec{t}_{\text{CT}}}_{\text{CT}} \Big) \quad (32)$$

Here, the effect of the CT state on the polarization $\vec{P}^\beta$ of the mixed exciton states is clearly visible: Without consideration of a finite CT transition dipole ($p^{\text{rel}}_{\text{CT}} = 0$), all states are polarized along the direction $\vec{t}_{\text{ME}}$. In this case, the CT mixing causes only the appearance of an additional absorbing exciton state. The redistribution of the Frenkel exciton transition dipole to all states is depicted by the notion that the CT exciton 'borrows' its oscillator strength from the Frenkel states. In the case of a finite CT transition dipole ($p^{\text{rel}}_{\text{CT}} > 0$), an additional component appears. If $\vec{t}_{\text{CT}}$ contains a component perpendicular to $\vec{t}_{\text{ME}}$, the contribution of the CTE in each exciton state could be directly seen in an absorption spectrum with light polarized along this perpendicular component.

Up to now, the model was strictly one-dimensional. A realistic three-dimensional crystal consists of a two-dimensional array of weakly interacting one-dimensional stacks. The macroscopically observable polarization is the net effect of all one-dimensional stacks. In a crystal with only one molecule per unit cell, all one-dimensional stacks have the same orientation and the transition dipole (32) of a 1D-exciton state can be directly probed by polarized light. MePTCDI and PTCDA crystals, however, contain two molecules per unit cell, which form two non-equivalent one-dimensional stacks A and B. If we want to measure the polarization $\vec{P}^\beta(\text{A})$ of the exciton state β in stack A, we will also observe the contribution $\vec{P}^\beta(\text{B})$ from the other, non-equivalent stack B.

Now, two cases have to be distinguished. If the interaction between the stacks is sufficient to cause coherently coupled exciton states, two Davydov components with different energies and orthogonal polarization $\vec{P}^\beta_{p/s}$ will be formed:

$$\vec{P}^\beta_{p/s} = \sqrt{N_2}\, \frac{\vec{P}^\beta(\text{A}) \pm \vec{P}^\beta(\text{B})}{\sqrt{2}} \,, \quad (33)$$

where $2N_2$ is the number of stacks. The oscillator strength of a state with energy E and transition dipole $\vec{P}$ is $F = 2m/(e^2\hbar^2) \cdot E|\vec{P}|^2$ (in cgs-units). With (32) and (33), the directly observable oscillator strength for light polarized along the p and s directions of the Davydov components are therefore given by:

$$\begin{aligned} F^\beta_{p/s} = \frac{mN_2N}{e^2\hbar^2} p^2_{\text{ME}} E^\beta \cdot \Big| & U_{\beta(k=0)} \big[\vec{t}_{\text{ME}}(\text{A}) \pm \vec{t}_{\text{ME}}(\text{B})\big] \\ & c_{\beta(k=0)} p^{\text{rel}}_{\text{CT}} \big[\vec{t}_{\text{CT}}(\text{A}) \pm \vec{t}_{\text{CT}}(\text{B})\big] \Big|^2 \end{aligned} \quad (34)$$

If, however, the interaction between the stacks is too weak to create coherently coupled states (oriented gas model), a polarized light beam will probe the components of each 1D-state

independently. Let us consider light polarized within the plane spanned by $\vec{P}^{\beta}(\mathrm{A})$ and $\vec{P}^{\beta}(\mathrm{B})$. We now rotate the polarization in this plane. If the angle between $\vec{P}^{\beta}(\mathrm{A})$ and $\vec{P}^{\beta}(\mathrm{B})$ is $< 45°$ ($> 45°$), the absorption will have a maximum (minimum) in the p-direction given by $\vec{P}^{\beta}(\mathrm{A})+\vec{P}^{\beta}(\mathrm{B})$ and a minimum (maximum) in the s-direction given by $\vec{P}^{\beta}(\mathrm{A})-\vec{P}^{\beta}(B)$. Adding the effective components of the oscillator strength gives for both directions the same result that is obtained for the two Davydov components in the case of coherent coupling. Therefore, equation (34) gives the correct oscillator strength for both coherent and incoherent inter-stack coupling. The difference between the two regimes is exclusively expressed by the peak positions for the two polarization directions: Only in the case of coherent coupling, the absorption maxima for p- and s-polarized light occur at a different energy (Davydov splitting).

For a general investigation of the polarization behavior, all four directions $\vec{t}_{\mathrm{ME}}(\mathrm{A/B})$ and $\vec{t}_{\mathrm{CT}}(\mathrm{A/B})$ would have to be considered. For simplification, we will discuss only the polarization in the plane spanned by $\vec{t}_{\mathrm{ME}}(\mathrm{A})$ and $\vec{t}_{\mathrm{ME}}(\mathrm{B})$. The polarization of a pure Frenkel state lies exclusively in this plane, which we will henceforth call the 'FE-plane'. If the CT transition dipoles have components perpendicular to the FE-plane, these components can be directly observed as out-of-plane components. If, however, the CT transition dipoles lie in the FE-plane, their contribution is only indirectly accessible. As will be described in section 5, this latter case is approximately realized in MePTCDI and PTCDA. Let $\vec{t}'_{\mathrm{CT}}(\mathrm{A/B})$ be the projections of $\vec{t}_{\mathrm{CT}}(\mathrm{A/B})$ on the FE-plane. Then, the substitution $\vec{t}_{\mathrm{CT}} \rightarrow \vec{t}'_{\mathrm{CT}}$ gives in (32) the component $\vec{P}'^{\beta}$ of the 1D-stack exciton in the FE-plane, and in (34) the measurable oscillator strength $F'^{\beta}_{p/s}$ for light polarized in the FE-plane.

The polarization ratio in the FE-plane is defined as

$$R'^{\beta} = \frac{F'^{\beta}_{p}}{F'^{\beta}_{s}} \,. \tag{35}$$

This polarization ratio is the observable expression of the exciton polarization in the FE-plane. If $p^{\mathrm{rel}}_{\mathrm{CT}} = 0$ it greatly simplifies and becomes

$$R_0 = \frac{\cos^2\varphi}{\sin^2\varphi} \,,$$

where φ is the angle between $\vec{t}_{\mathrm{ME}}(\mathrm{A})$ and $\vec{t}_{\mathrm{ME}}(\mathrm{B})$. Remarkably, R_0 is the same for all these vibronic exciton states since all Frenkel states have the same polarization $\vec{t}_{\mathrm{ME}}$. The finite value of R_0 for $\varphi \neq 0$ expresses the fact that there is absorption for all light polarizations in the FE-plane due to the two non-equivalent molecules. Therefore, an additional CT transition dipole in the FE-plane will not appear as a completely new component but will only influence the polarization ratio. Although R_0 is well defined by the crystal structure, an experimental deviation from R_0 could also arise if the measurement was not performed precisely in the FE-plane or if the sample consisted of crystallites with imperfect orientation. However, both these experimental imperfections would lead to a constant polarization ratio for all considered states. On the other hand, a CT contribution with $p^{\mathrm{rel}}_{\mathrm{CT}} > 0$ will vary for the various mixed states ($c_{\beta} \neq \mathrm{const}$) and will therefore lead to a varying polarization ratio. This variation of R'^{β} as a function of the band index β is the observable consequence of the admixed CT transition dipole.

Thus, we can expect two main effects from the Frenkel-charge-transfer mixing in our model Hamiltonian: (i) If the coupling constant ϵ_+ is in the same order as the energetic separation between the CTE and at least one of the $\nu_{\max}$+1 vibronic Frenkel states, the model predicts a strong mixing resulting in $\nu_{\max}$+2 significantly absorbing states. (ii) With a finite CT transition dipole (not parallel to the molecular dipole), the polarization direction of the states will vary due to the varying composition of the bands. In a three-dimensional crystal with two molecules per unit cell, this will lead to a variation of the polarization ratio R'^{β} as a function of the band index β.

IV. MEASUREMENT OF ABSORPTION SPECTRA

Absorption spectra were obtained and analyzed in the following way: All spectra are given as the optical density of the whole sample: $\mathrm{O.D.} = -\log_{10}$ (transmitted intensity / incident intensity). The organic dyes were commercially purchased (MePTCDI from Syntec, Wolfen; PTCDA from Aldrich) and purified by gradient sublimation. For obtaining solution spectra at well defined concentrations, an indirect method was used because of the extremely low solubility of the materials. In order to dissolve a measurable amount of material, we first vapor-deposited a thin film onto a polymer substrate (commercial cellulose acetate film base, Filmfabrik Wolfen, Germany) behind a well-defined mask. This dye-covered substrate was then dissolved in chloroform (for MePTCDI) or DMSO (dimethyl-sulfoxide, for PTCDA) and the solution further diluted. Optical density spectra were measured of this solution, and the spectra of a reference solution with a dissolved blank substrate were subtracted. Then, films were vapor-deposited onto glass substrates under identical conditions. The films on the glass substrates were dissolved in conc. H_2SO_4 and measured like the films on the polymer substrate. The solution spectra in H_2SO_4 are strongly red shifted compared to chloroform or DMSO, but still show the distinct chromophore absorption. Now, the concentration of the H_2SO_4 solutions, which is equal to the unknown concentration in the organic solvents, can be determined: Due to the much higher solubility in H_2SO_4, 10 mg of the dyes could be reproducibly dissolved in 50 ml H_2SO_4 and then diluted to a similar concentration like the solutions from the vapor-deposited film.

The solution spectrum of MePTCDI in chloroform is shown in Fig. 2a. The spectrum of PTCDA in DMSO looks almost identical. We note that for MePTCDI in solution the concentration dependence is similar as discussed in [19] for PTCDA: At concentrations higher than 2 μmol/l, a new peak at 2.16 eV appears, which is due to the formation of aggregates. From the monomeric solvent spectra (Fig. 2a) we obtained the oscillator

strength by (e.g. [43], p.9):

$$f_{\mathrm{sol}} = 4.319 \cdot 10^{-9} \int \epsilon_{\tilde{\nu}} d\tilde{\nu}, \tag{36}$$

where $\epsilon_{\tilde{\nu}}$ is the decadic molar extinction coefficient in $\mathrm{l}/(\mathrm{mol}\cdot\mathrm{cm})$ and $\tilde{\nu}$ the wave number in cm^{-1}. By integrating over the intense bands ($2.2 - 3.1\,\mathrm{eV}$) we obtain the oscillator strength (in solution) of the S_0-S_1-transition (MePTCDI: 0.53, PTCDA: 0.65) and by integration over the weak structure at $3.1 - 3.6\,\mathrm{eV}$ the oscillator strength of the S_0-S_2-transition (MePTCDI: 0.052).

In order to account for the local field effects caused be the solvent, we used the simple correction

$$f_{\mathrm{gas}} = f_{\mathrm{sol}} \cdot n_0 \left(\frac{3}{n_0^2 + 2} \right)^2 , \tag{37}$$

where n_0 is the refractive index of the solvent at the considered frequency. This correction corresponds to the model of a hollow sphere in a dielectric continuum (application to solution spectra e.g. in [43], p. 100) or to the model of a substitutional impurity in an isotropic crystal ([39], p.56). With application of (37), we obtain the gas-phase oscillator strengths and with $p^2 = 3he^2/(8\pi^2 mc\tilde{\nu}) f_{\mathrm{gas}}$ ([43], p. 58) the gas-phase transition dipoles for the S_0-S_1-transition (MePTCDI: $p_1 = (6.8 \pm 0.7)\mathrm{Debye}$, PTCDA: $p_1 = (7.4 \pm 0.7)\mathrm{Debye}$) and for the S_0-S_2-transition (MePTCDI: $p_2 \approx 1.8\,\mathrm{Debye}$).

These values contain considerable uncertainties. The statistical error of our procedure we estimate to be 20% for the oscillator strength. The correction for vacuum values can be very uncertain, too ([43], p. 100). Furthermore, the S_0-S_2 absorption lies hardly above the background level. A considerably higher value of f_{sol}=1.0 for the MePTCDI S_0-S_1 transition in chloroform is reported in [44]. For our purposes, these uncertainties are not critical since we only need the appropriate order of magnitudes for the estimations in section 5.

From the solution spectra, the vibrational spacing $\hbar\omega$ and the vibronic overlap factors s_ν according to (11) can be obtained: Therefore, the spectra were fitted by a sum of four Gaussians. The relative oscillator strength of each peak, i. e., its Franck-Condon factor $F_{0\nu}$ can be expressed with the exciton-phonon-coupling constant g by [45]:

$$F_{0\nu} = |\langle \chi^{1\nu} | \chi^{00} \rangle|^2 = \frac{g^{2\nu}}{\nu!} \mathrm{e}^{-g^2} \tag{38}$$

With (38), g and thereby the overlap factors s_ν can be derived from the relative oscillator strengths of two levels. We evaluated the first two levels ($\nu = 0, 1$) to obtain $\hbar\omega$ and s_0, s_1. The overlap factor s_2 was calculated in the same way by relating the level $\nu = 2$ to the zero level. This results in a spacing $\hbar\omega = 0.17\,\mathrm{eV}$ (MePTCDI and PTCDA) and overlap factors $s_0 = 0.64$, $s_1 = 0.60$, $s_2 = 0.36$ (MePTCDI) or $s_0 = 0.62$, $s_1 = 0.61$, $s_2 = 0.37$ (PTCDA).

For obtaining crystal spectra, thin films were grown by physical vapor deposition in high vacuum ($p < 10^{-3}\,\mathrm{Pa}$) from indirectly heated quartz glass crucibles. The film thicknesses were $\approx 100\,\mathrm{nm}$ and the deposition rate was kept at $\approx 0.2\,\mathrm{nm/s}$. As substrate, we used a polymer film (PETP, polyethylene terephthalate) which was produced as a commercial photographic film base (Filmfabrik Wolfen, Germany). Such a film is stretched during the production first in the longitudinal and then in the transverse direction ([47], p. 65). Substrate temperatures during the deposition process were varied between $-170\,^{\circ}\mathrm{C}$ and $+100\,^{\circ}\mathrm{C}$. For all substrate temperatures, films of PTCDA were optically homogeneous (down to a length scale of several $\mu\mathrm{m}$) and showed no azimuthal polarization dependence. For MePTCDI, the films appear inhomogeneous and their absorption varies with the azimuthal polarization direction. The largest polarization ratio, i.e, the strongest anisotropy, was found for films produced at approximately room temperature. Therefore, all investigations presented here were done at films grown at room temperature.

The films of MePTCDI, which appear inhomogeneous to the naked eye, consist of domains with irregular shape and sizes of $1 - 1000\,\mu\mathrm{m}$. A few of these domains have a clear rectangular shape, a very homogeneous absorption (at $1\,\mu\mathrm{m}$ resolution), a high polarization ratio and the direction of their maximum absorption lies parallel to the transverse stretching direction of the polymer substrate. Such domains were chosen for microscopic polarized absorption measurements. From atomic force microscopy, it could be shown that these domains, in spite of their optical homogeneity, still consist of microcrystals of $\approx 100\,\mathrm{nm}$ diameter.

For low temperature measurements, the samples were cooled in a helium cryostat with gaseous helium at ambient pressure in the sample compartment. The temperature ($5\,\mathrm{K}$) was measured at the sample holder. The spectra were only weakly dependent on the temperature and gradually broaden at temperatures above $\approx 20\,\mathrm{K}$. The sample was illuminated with a halogen lamp through a blue colored filter for spectral adaption. Several lenses and apertures were set up as an imaging system, which allowed to direct the light selected from an area of typically $5 \times 5\,\mu\mathrm{m}^2$ into the entrance slit of a spectrograph. A polarizing filter was installed between the sample and the spectrograph. The optical density was determined from two consecutive light intensity measurements with a diode array, the first with the sample and the second after removing the sample. This set-up was successfully tested by comparing the spectra of the homogeneous and isotropic PTCDA films measured at room temperature with measurements in a commercial spectro-photometer (UV-2101/3101PC, Shimadzu). The spectral resolution of the set-up was experimentally checked with a HeNe laser and amounted to $1\,\mathrm{nm}$.

With this set-up, the optical density of the PTCDA film and of domains in the MePTCDI film was measured for the polarization directions of maximum and minimum absorption (p and s direction, resp.). These optically determined polarization directions correspond to the transverse and longitudinal stretching directions of the film base substrate. Then, the optical density of a pure substrate was subtracted. The spectrum of PTCDA does not depend on the polarization and is shown in Fig. 2c. For MePTCDI, the spectra for the two polarization directions are given in Fig. 4. At room temperature, the spectra of MePTCDI look qualitatively similar to the absorption

spectra of the microcrystal dispersion [46] to which the crystal structure analysis [30] is correlated. Also, we have never observed phase transitions (such as between α- and β-copperphthalocyanine) in the absorption spectra for films grown at varying substrate temperatures ($-170\,^\circ\mathrm{C}\ldots+100\,^\circ\mathrm{C}$). X-ray diffraction measurements (see section 5) give the same (102) lattice plane spacing as in [30]. Therefore, we assume that our films consist of microcrystals with the crystal structure from [30]. For PTCDA we assume the α-phase crystal structure from [13–16].

For further application of the exciton model, all spectra were analyzed in terms of a four-band model. With neglect of frequency dependent damping, the transition dipole $\vec{P}^{\beta}_{p/s}$ determines the dielectric constant in the vicinity of the transition ([48], p. 360) and is therefore related to the spectroscopic quantity:

$$|\vec{P}^{\beta}_{p/s}|^2 \propto \int n\kappa \, dE \tag{39}$$

where n and κ are the real and imaginary part of the complex refractive index. The determination of the complex refractive index for thin organic layers requires more than one transmission measurement and was not possible for our small domains at low temperature. Such measurements were done for homogeneous and (in the film plane) isotropic films of MePTCDI at room temperature [49]. We now presume that n does not strongly depend on temperature and polarization and use the n values from [49]. Furthermore, we approximate the absorption coefficient $\mu = 2\kappa E/(\hbar c)$ to be proportional to the optical density of the sample. This approximation was checked to be very good for films of such thickness by comparing room temperature O.D. spectra with the optical constants from [49]. Obviously, reflection and multiple interference effects play a minor role in our case of rather large film thicknesses. Thus, a relative measured oscillator strength (peak intensity) can be evaluated as

$$\tilde{F}^{\beta}_{p/s} := n(E^{\beta}) \int \mathrm{O.D.}\, dE \; . \tag{40}$$

Now, the four predicted exciton bands have to be assigned to the peaks in the O.D. spectra. The high energy spectral region between $2.6\,\mathrm{eV}$ and $3.0\,\mathrm{eV}$ cannot be well described by one simple Gaussian. Therefore, we fitted the whole spectrum with a sum of five Gaussians (G1-G5), which is shown for the p polarized spectrum of MePTCDI in Fig. 3. The center position and total area of the Gaussians G1 - G3 are directly interpreted as experimental energies $\tilde{E}^{\beta}_{p/s}$ and intensities $\tilde{F}^{\beta}_{p/s}$ of exciton states. $\tilde{E}^{4}_{p/s}$ and $\tilde{F}^{4}_{p/s}$ of the highest exciton state is then assigned to the weighted average of the two Gaussians G4 and G5. We apply this somewhat artificial procedure in order to use a model with only four exciton bands. As will be discussed in section 5, the high energy region is expected to have a complicated structure. A detailed description of this structure is beyond the scope of this paper. The obtained peak positions and intensities are listed in Table 1. A graphic representation is given in Fig. 4 for the peak positions and experimental polarization ratios $\tilde{R}^{\beta} := \tilde{F}^{\beta}_{p}/\tilde{F}^{\beta}_{s}$. We applied the same procedure to the low-temperature absorption spectrum of PTCDA (shown in Fig. 2c) using optical constants determined as in [49].

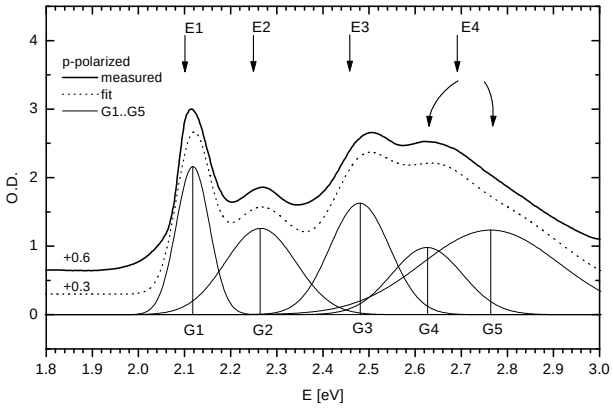

FIG. 3: Peak analysis for the p-polarized optical density spectrum of MePTCDI. The measured spectrum is fitted by a sum of five Gaussians (G1-G5). For the interpretation in a four-band-model, the weighted average of G4 and G5 is assigned to one exciton band at E4.

V. APPLICATION OF THE MODEL TO POLARIZED ABSORPTION SPECTRA

For an application of the model from section 3, we first consider only the polarized spectra of MePTCDI, which are shown in Fig. 4. The peak fitting results are summarized in Table 1 and the peak positions and polarization ratios are also visualized in Fig. 4. Already qualitatively it is obvious that the polarization ratio varies for the four peaks, which justifies the application of the model. Furthermore, a clear Davydov splitting in the order of $10-25\,\mathrm{meV}$ can be observed (cf. Table 1), which indicates a coherent coupling between the non-equivalent stacks. We will at first neglect this small splitting and apply the one-dimensional model.

Since the monomer absorption spectra (see Fig. 2a) show three significant peaks, we consider $\nu_{\max}+1 = 3$ levels $\Delta^{\nu}_{\mathrm{F}}$ of the molecular Frenkel exciton. Since the vibrational spacing $\hbar\omega$ of the monomer is not expected to change significantly in the crystal, the energy levels $\Delta^{\nu}_{\mathrm{F}}$ can be expressed by one parameter Δ^{0}_{F}:

$$\Delta^{\nu}_{\mathrm{F}} = \Delta^{0}_{\mathrm{F}} + \nu\hbar\omega \tag{41}$$

The on-site energy Δ^{0}_{F} of the lowest level differs from the value of the isolated molecule by the gas-to-crystal shift $\mathcal{D}$ and is therefore an unknown parameter. The further unknown parameters in the Hamiltonian matrix (25) at $k = 0$ are Δ_{CT}, M, and $|\epsilon_{+}|$. With these four parameters, the peak positions of the four exciton states are determined.

For a description of polarization dependent peak intensities in (34), $\vec{p}_{\mathrm{ME}}(\mathrm{A/B})$ and $\vec{p}_{\mathrm{CT}}(\mathrm{A/B})$ are additionally required. The direction $\vec{t}_{\mathrm{ME}}(\mathrm{A/B})$ is clearly given by the long molecular axes of the two molecules in the unit cell. The angle φ

TABLE I: Experimental results vs. model fit for MePTCDI. The experimental peak positions $\tilde{E}^\beta$, intensities $\tilde{F}^\beta$ and Davydov splittings $\Delta\tilde{E}^\beta$ are derived from a peak analysis described in section 4. All numbers are given in eV.

band No β	1	2	3	4
Exp: $\tilde{E}_p^\beta$, $\tilde{E}_s^\beta$	2.118 2.129	2.265 2.265	2.480 2.497	2.724 2.749
Model: E^β	2.112	2.292	2.491	2.644
Exp: $\tilde{F}_p^\beta$, $\tilde{F}_s^\beta$	0.392 0.095	0.463 0.156	0.507 0.108	0.965 0.233
Model: F_p^β , F_s^β	0.289 0.062	0.166 0.060	0.629 0.123	2.042 0.338
Exp: $\Delta\tilde{E}^\beta$	-0.011	0.000	-0.017	-0.025
Model: ΔE^β	-0.011	-0.005	-0.019	-0.050

between $\vec{t}_{\mathrm{ME}}(\mathrm{A})$ and $\vec{t}_{\mathrm{ME}}(\mathrm{B})$ derived from the crystal structure [30] amounts to $\varphi = 36.8°$. The directions $\vec{t}_{\mathrm{CT}}(\mathrm{A/B})$ of the CTE are discussed in the Appendix. Within an individual stack, $\vec{t}_{\mathrm{CT}}$ lies approximately in the molecular plane and makes an angle of $\gamma = 68°$ with the long molecular axis. With knowledge of these directions, only the absolute values p_{ME} and $p_{\mathrm{CT}}^{\mathrm{rel}}$ remain as unknown parameters of the model.

For simplification, we will now only consider the polarization behavior in the FE-plane spanned by the molecular transition dipoles, as it is discussed in section 3. This plane can be well approximated by the (102) plane of the crystal, because in MePTCDI and especially in the well-known case of PTCDA the molecules lie approximately in the (102) plane: The molecular N-axis (normal to the molecular plane) deviates by only $\approx 10°$ from the [102] direction (derived from [30]) in MePTCDI and $\approx 5°$ in PTCDA [52]. Furthermore, also the CT transition dipoles $\vec{p}_{\mathrm{CT}}(\mathrm{A/B})$, which are roughly parallel to the molecular planes, lie in this FE-plane approximated by the (102) crystal plane. Therefore, we do not explicitly consider the projection $\vec{t}'_{\mathrm{CT}}$ of the CT transition directions on the FE-plane but directly use equation (34) for the oscillator strength in the (102) plane.

In our investigated thin films, the (102) plane lies preferentially parallel to the substrate plane, and the measured polarized spectra directly probe the transition dipoles of the predicted exciton states. This preferential orientation is concluded from X-ray diffraction measurements and supported by the polarization behavior of the S_0-S_2 transition: X-ray measurements of an $\approx 100\,\mathrm{nm}$ thick film in Bragg-Brentano geometry show only one peak corresponding to a lattice plane distance of (3.23 ± 0.01) Å. According to the published crystal structure [30], we assign this peak to the (102) lattice planes ($d_{102} = 3.22$ Å). Rocking curve measurements of the (102) peak (cf. [50] for PTCDA) give a rocking width of about 7° FWHM for tilting the sample in both the p or the s direction. Although narrower rocking curves are possible for well ordered organic films (e.g. $0.3°$ for PTCDA on GeS(010) [50]), the finite rocking width in our samples proves that for the majority of the crystallites the (102) plane makes only a small angle with the substrate plane (for $\approx 95\,\%$ within $\pm 2\sigma = \pm 6°$).

Further confirmation is provided by the polarization behavior of the M-axis polarized S_0-S_2 transition, which does not significantly mix with the S_0-S_1 transition (see below). The spectral region of this transition could only be measured at room temperature without spatial resolution and is shown for the s-direction in Fig. 2b. Compared to the intensity ratio of the isotropically oriented monomer in solution, the S_0-S_2 peak is greatly enhanced with respect to the S_0-S_1 absorption structure for this polarization. For the p direction, the S_0-S_1 intensity increases and the S_0-S_2 intensity decreases. That means, that both the long-axis transition S_0-S_1 and the M-axis transition S_0-S_2 must have a considerable component in the substrate plane. A quantitative evaluation is not possible, since the S_0-S_2 intensity is too weak compared to the unidentified ground level in this region and due to the unknown influence of an anisotropic refractive index. Both X-ray diffraction and these polarization data demonstrate that the (102) plane of the MePTCDI crystallites lies parallel to the substrate. Such a growth mode is very common for PTCDA and it is also observed for MePTCDI on KCl at $+100\,°\mathrm{C}$ [51].

Thus, both molecular and CT transition dipoles lie approximately parallel to the substrate plane, and the peak intensities $\tilde{F}_{p/s}^\beta$ (cf. Table 1) derived from the polarized absorption spectra can be directly related to the model transition dipoles from equation (34). After collecting all multiplicative constants in $F_0 := mN_2N/(e^2\hbar^2)\cdot p_{\mathrm{ME}}^2$, the model intensities according to (34) are given by six unknown model parameters: Δ_{F}^0, Δ_{CT}, M, $|\epsilon_+|$, $p_{\mathrm{CT}}^{\mathrm{rel}}$, and F_0. In order to see if the experimental results can be reasonably described by an appropriate parameter set, we considered all these parameters as fitting parameters. With an optimization routine that minimizes the weighted deviations for peak positions, intensities and polarization ratios, the best description of the physical situation is obtained with the following model parameters: $\Delta_{\mathrm{F}}^0 = 2.23\,\mathrm{eV}$, $\Delta_{\mathrm{CT}} = 2.15\,\mathrm{eV}$, $M = 0.11\,\mathrm{eV}$, $|\epsilon_+| = 0.10\,\mathrm{eV}$, $p_{\mathrm{CT}}^{\mathrm{rel}} = 0.26$, and $F_0 = 0.40$. The peak positions and intensities that follow from these parameters are compared to the experimental values in Table 1. A graphic comparison between model fit and experiment is shown in Fig. 4 for the peak positions and polarization ratios R^β, which are the physically most relevant values.

The first three peaks are in good agreement with the experimental spectra. Especially, the relatively small polarization ratio of the second peak at $2.26\,\mathrm{eV}$ is well described. This peak is most strongly affected by the CT exciton. Only for the fourth peak at $2.72\,\mathrm{eV}$, model and experiment deviate considerably. This discrepancy is not surprising since already the peak analysis of the spectra has shown that several transitions contribute to this part of the spectrum. Here we reach the limits of our simple four-band model: In reality, the very closely spaced vibronic modes of the isolated molecule, which are treated as one effective mode in the monomer spectrum, will spread over a wider energy range as a result of Frenkel exciton transfer. Furthermore, this higher energy region will be affected by the so far neglected vibronic replicas of the CT exciton. This explains why the experimental polarization ratio of the fourth peak is much lower than the model prediction.

The model parameters obtained from the fit represent qualitatively the same scenario as derived from the quantum chemical calculations (see Appendix). Especially the parameter for the Frenkel-CTE-mixing $|\epsilon_+| = 0.10\,\mathrm{eV}$ agrees reasonably

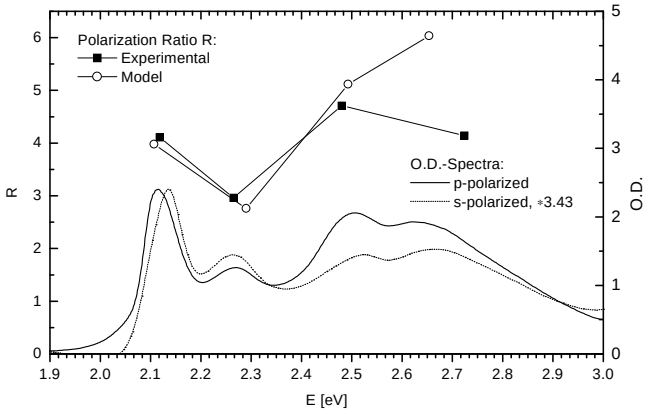

FIG. 4: Comparison of experimental polarized absorption spectra of MePTCDI with the exciton model. The polarization ratios (from the peak analysis) also indicate the peak positions for the p-direction. The s-polarized spectrum is scaled for easier comparison; the Davydov-splitting is most clearly seen for the lowest peak. The model predicts similar peak positions and for the lowest three states comparable polarization ratios.

well with the quantum chemical result of $0.16\,\mathrm{eV}$, and a high contribution of the CTE-transition dipole ($p_{\mathrm{CT}}^{\mathrm{rel}} = 0.27$) is also supported by the quantum chemical result of 0.19. Since transition dipoles scale with the orbital overlap, the large value of $p_{\mathrm{CT}}^{\mathrm{rel}} = 0.27$ nevertheless seems an overestimation due to the global fit. An improved model with all vibronic states and without approximation (14) might give a better description of the oscillator strengths with a different value of $p_{\mathrm{CT}}^{\mathrm{rel}}$. The obtained Frenkel exciton transfer constant $M = 0.11\,\mathrm{eV}$ is also reasonable: Using the point-dipole approximation for the molecular transition dipole $p_1 = 6.8\,\mathrm{Debye}$ (from the solution spectrum) and neglecting dielectric screening, a transfer integral of $M_{\mathrm{vac}} = 0.41\,\mathrm{eV}$ is obtained. The difference between M and M_{vac} corresponds to an effective dielectric screening constant at this frequency of $\epsilon_{\mathrm{eff}} = 3.7$. This seems very plausible compared to the dielectric constant of 4.1 from [53], which was determined for (102) plane polarization of PTCDA at $1.16\,\mathrm{eV}$, i.e. below the considered exciton transition.

Interestingly, the model fit yields an energetic position of the localized CTE *below* the molecular excitation ($\Delta_{\mathrm{CT}} < \Delta_{\mathrm{F}}^{0}$). Thus, the nature of the lowest absorption peak is essentially of charge-transfer parentage. Such a result is counterintuitive for one-component molecular crystals: In a simple picture, the transition from the Frenkel exciton to the CTE means a charge separation, which requires energy. This picture, however, is misleading if the separation between the molecules (e.g. $3.4\,\text{Å}$ between the molecular planes in MePTCDI) becomes smaller than the size of the conjugated system (e.g. N-N′-distance in MePTCDI: $11.3\,\text{Å}$). In this case, there is no simple way to consider the molecular excitation as an electron-hole pair with a separation smaller than for the CTE. Further effects arise from the strong polarizability of the surrounding crystal. Therefore, there is no general rule concerning the relative positions of molecular and charge-transfer excitations [7, 54]. A CTE position *above* the molecular excitation is suggested in [17] (from a fit of the PTCDA absorption spectra) and in [55] (from calculations of the absolute CT energies). The same follows from our quantum chemical calculations, but these are certainly not accurate enough. Since the assignment of the CTE in our model fit also depends on the simplified description of the higher energy region, a definite conclusion can not be drawn yet. However, this does not affect the central message of a strong mixing between Frenkel and CT states due to their energetic proximity.

Only quantum chemistry can provide the parameter ϵ_-, which is not accessible from absorption experiments. With ϵ_-, the full momentum dependent band structure for the excitons can be calculated. In order to give a qualitative picture, we scaled $\epsilon_\pm$ from the quantum chemical calculations so that ϵ_+ corresponds to the model fit: $|\epsilon_-| = 0.29|\epsilon_+|$. The resulting band structure is shown in Fig. 5b. There, the composition of the bands is also indicated by a schematic visualization of the k-dependent values $|U_\beta(k)|^2$ from (28) and $|c_\beta(k)|^2$ defined by (24). $|U_\beta(k)|^2$ represents the total fraction of all Frenkel states weighted by their contributing transition dipoles, whereas $|c_\beta(k)|^2$ directly gives the contribution of the CT exciton. The Γ-point ($k = 0$) of this band structure represents the states accessible by optical absorption. For easy comparison, in Fig. 5a the absorption spectrum is shown again at the same energy scale. The upper shaded stripe at each band representing $|U_{\beta(k=0)}|^2$ gives the main part of the oscillator strength. The lower shaded stripes show the coefficients $|c_{\beta(k=0)}|^2$ of the charge-transfer exciton, which have to be multiplied by the factor $|p_{\mathrm{CT}}^{\mathrm{rel}}|^2 = 0.07$ to get the contributing CTE oscillator strength (cf. (32)).

Since the bottom of the proposed band structure lies at the edge of the Brillouin zone, luminescence is expected to appear as a weak, indirect transition from these $k = \pi$ states (as also discussed in [17]). In Fig. 5c, we show an experimental transient emission spectrum (time window $0 - 40\,\mathrm{ps}$) after a short pulse excitation at $2.77\,\mathrm{eV}$. Interestingly, the bottom of the proposed band structure coincides with a small emission feature at $2.10\,\mathrm{eV}$, which has a short lifetime below the time resolution of $\approx 10\,\mathrm{ps}$. All lower emission peaks have a multi-exponential decay time on time scales in the order of $1\,\mathrm{ns}$. These features coincide with the typical cw emission spectrum (as for PTCDA in [17]). The long-lived states might be identified with self-trapped excitons or emission from defects. Thus, we suggest that the main emission as observed in cw-luminescence spectra does not result directly from the bottom of the band structure but occurs only after further relaxation processes. For one-dimensional crystals, exciton self-trapping is strongly expected [1]. Also, effective exciton migration to lower lying defect states is very common in organic crystals (as for example X-trap emission in anthracene [56]).

We emphasize that the proposed band structure results entirely from the absorption fit *and* the quantum chemically calculated parameter ϵ_-. Our approach is different from the one used for PTCDA in [17], where the bottom of the lowest exciton band is fixed to the cw-emission spectrum. This explains the smaller dispersion in our band structure (mainly expressed by a smaller exciton transfer integral $M = 0.11\,\mathrm{eV}$ instead of $0.18\,\mathrm{eV}$). Still, the qualitative situation of a strong Frenkel-CT-mixing in the lowest band is similar.

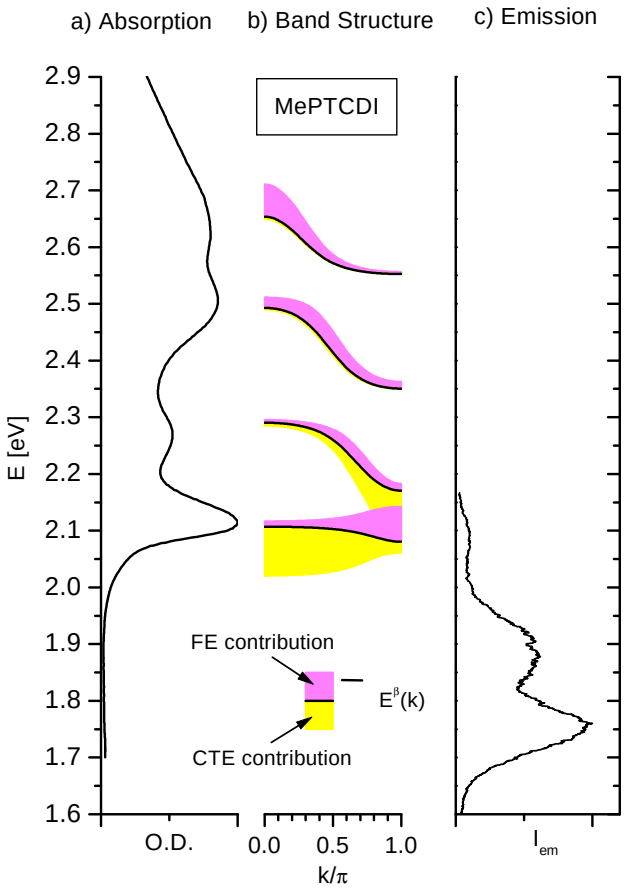

FIG. 5: Scheme of the exciton band structure in MePTCDI. a) p-polarized absorption spectrum at 5 K. b) Dispersion of the mixed exciton bands $E^{\beta}(k)$, $\beta = 1 \ldots 4$ (solid lines). The upper, dark shaded stripes show the contribution of the Frenkel exciton states given by $|U_{\beta}(k)|^2$. The lower, light shaded stripes show the contribution of the charge-transfer exciton given by $|c_{\beta}(k)|^2$. c) Transient emission spectrum of a poly-crystalline MePTCDI film at 5 K (time window $0 - 40$ ps after short pulse excitation, streak-camera measurement, no correction for spectral instrument response). The highest peak at about 2.1 eV has a live time < 10 ps, the two lower peaks decay multi-exponentially on time scales of ≈ 1 ns.

So far, the observed polarization dependence has been interpreted as a result of the mixing with the CT exciton. This argumentation is only valid if mixing with higher, M-axis polarized molecular transitions can be excluded. We now give an estimation for the importance of such mixing. For simplification, we consider only two purely electronic molecular transitions: the long axis polarized lowest molecular S_0-S_1 transition and the next highest, M-axis polarized S_0-S_2 transition. The mixing between the S_1 and S_2 states is determined by the transfer integral M_{1-2} for excitation transfer from the S_1 state to the S_2 state at the nearest-neighbor in the stack. In point-dipole approximation without screening, we obtain from the molecular transition dipoles p_1 and p_2: $M_{1-2} = 0.04\,\mathrm{eV}$. This value is considerably smaller than the energetic difference between the exciton states created from S_1 and S_2, which can be estimated from the crystal spectra to be $\Delta E_{1-2} > 0.5\,\mathrm{eV}$. Therefore, the two states mix only weakly and the relative admixture of the S_2-transition dipole to the S_1-dipole is in the order of $p^{\mathrm{rel}}_{1-2} \approx M_{1-2}/\Delta E_{1-2} \cdot p_2/p_1 < 0.02$.

This estimate is a rough upper limit, which would be further reduced if the lower vibronic S_1 bands, more accurate transition dipoles and especially screening effects in the point-dipole approximation were considered. Nevertheless, p^{rel}_{1-2} is already an order of magnitude smaller then the assumed contribution of the CTE transition dipole $p^{\mathrm{rel}}_{\mathrm{CT}}$. For higher molecular states polarized along the molecular M-axis, the energetic separation would be much larger and the mixing with the S_1 state even smaller. Therefore, the observed components $\vec{p}_{\mathrm{CT}}$ in the exciton states can not be caused by mixing with higher *intra*molecular configurations but must be due to the mixing with CT excitons.

Finally, we want to consider the additional effects due to Davydov splitting. A splitting of the peak-positions for the two polarization directions is qualitatively seen already in Fig. 4; the values derived from the peak analysis are given in Table 1. Since the shift of the peak positions due to this splitting is small compared to the accuracy of our model, the interaction between stacks and the distinction between coherent or incoherent inter-stack coupling was not important for our one-dimensional model. In order to calculate the three-dimensional exciton states with consideration of inter-stack coupling, three-dimensional interaction sums would be needed. Anisotropic screening effects would introduce several unknown parameters. Therefore, we give only a very simplified estimation: First, we neglect the contribution of CTE since it is a relatively small correction to the effective transition dipole of each exciton band. Second, we treat all interactions in point-dipole approximation. Third, we consider the screening effects by dividing all point-dipole interactions by one effective dielectric constant ϵ_{eff}. For this, we use the value $\epsilon_{\mathrm{eff}} = 3.7$, which was obtained from the screening for the nearest-neighbor interaction within the 1D-stacks. Fourth, we neglect interactions between the various exciton bands. Then, the Davydov splitting ΔE^{β} for each band can be calculated as in the standard three-dimensional two-level exciton problem ([38], p. 44) for two non-equivalent molecular transition dipoles $U_{\beta}\vec{p}_{\mathrm{ME}}(\mathrm{A/B})$. Here, the factor $U_{\beta(k=0)}$ describes how the electronic molecular transition dipole is distributed over the four exciton bands. For directions of $\vec{k}$ in the a-c-plane of the crystal or perpendicular to it, the Davydov splitting is then given by

$$\Delta E^{\beta} = \lim_{\vec{k}\to 0} {\sum_{\vec{n}}}' M_{0\mathrm{B},\vec{n}\mathrm{A}} \mathrm{e}^{\mathrm{i}\vec{k}\vec{n}}, \qquad (42)$$

where $M_{0\mathrm{B},\vec{n}\mathrm{A}}$ is the point-dipole interaction between a dipole $U_{\beta}\vec{p}_{\mathrm{ME}}(\mathrm{B})$ in the unit cell 0 and a dipole $U_{\beta}\vec{p}_{\mathrm{ME}}(\mathrm{A})$ in the unit cell $\vec{n}$ of the three-dimensional crystal.

The sum in (42) can be carried out directly for a small number of interactions or has to be evaluated by the Ewald method ([57], p. 248) for considering a macroscopic interaction volume. In both cases it reduces to

$$\Delta E^{\beta} = M^{\beta}_{\mathrm{AB}} Q_{\mathrm{AB}}(\vec{k}) \,, \qquad (43)$$

where M^{β}_{AB} is the interaction between molecules A and B in the same unit cell and $Q_{\mathrm{AB}}(\vec{k})$ is a lattice sum, which depends only on the crystal structure. The convergence behavior of the lattice sum is complicated and its limit for $\vec{k} \to 0$ depends on the direction of $\vec{k}$. For the crystal structure of MePTCDI, this spatial dispersion is dramatic if we consider infinite interaction sums calculated by the Ewald method: Then $Q = +33.7$ for $\vec{k} \parallel \vec{a}^{\,*}$, $Q = -25.7$ for $\vec{k} \parallel \vec{b}^{\,*}$ and $Q = +34.1$ for $\vec{k} \parallel \vec{c}^{\,*}$ where $\vec{a}^{\,*}, \vec{b}^{\,*}, \vec{c}^{\,*}$ are the reciprocal lattice vectors ($\vec{a}^{\,*}$ along the stacking direction). If we carry out the sum (42) only for small interaction volumes and a small $|\vec{k}|$ corresponding to the momentum of the exciting light, we obtain values which do not depend critically on the direction of $\vec{k}$ or the radius of summation: For all three directions and summation ranges between 3 and 20 lattice constants, the values of Q differ by less then 2.7%. We will use the value of $Q = +27.0$, which represents a summation range of three lattice constants and $\vec{k} \parallel \vec{a}^{\,*}$. This value is already close to the Ewald limit and represents approximately the experimental $\vec{k}$ direction. The obtained values for ΔE^{β} are compared to the experimental results in Table 1. Their order of magnitude and the general trends agree well. We conclude that the observed splitting of the peak positions is indeed the result of Davydov splitting caused by coherent coupling of the one-dimensional exciton states.

For PTCDA, the application of our model is much less reliable. We could not obtain samples that show polarized absorption spectra. This difficulty is not surprising since in PTCDA the two non-equivalent molecules in PTCDA make a large angle of $\varphi = 82°$, so that the crystal itself is less anisotropic than in the case of MePTCDI. Furthermore, the peaks in the absorption spectra (Fig. 2) are not as well separated. The evaluation of M depends strongly on the resolved peak structure, and $p^{\mathrm{rel}}_{\mathrm{CT}}$ on the polarization dependence. Therefore, we used for both the values from MePTCDI. Point-dipole approximation (for M) and quantum chemistry (for M and $p^{\mathrm{rel}}_{\mathrm{CT}}$) suggest similar values for both materials. The fitting procedure yields for the remaining parameters $\Delta^0_{\mathrm{F}} = 2.34\,\mathrm{eV}$, $\Delta_{\mathrm{CT}} = 2.27\,\mathrm{eV}$, $|\epsilon_+| = 0.10,\mathrm{eV}$, and $F_0 = 0.37$. With $|\epsilon_-| = 0.79|\epsilon_+|$ from the quantum chemical analysis for PTCDA, we obtain the exciton band structure shown in Fig. 6. The qualitative physical picture is very similar to the case of MePTCDI.

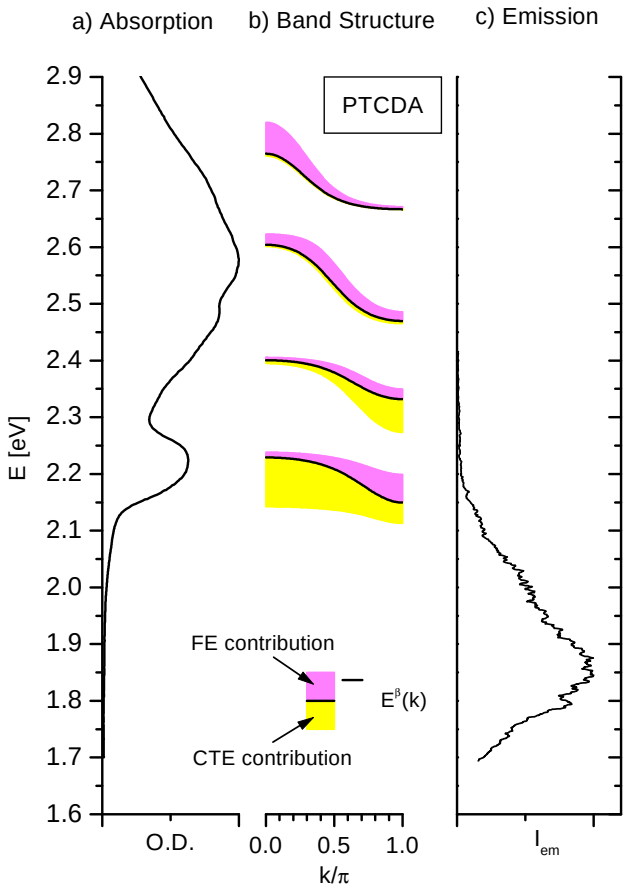

FIG. 6: Scheme of the exciton band structure in PTCDA. a) Absorption spectrum at 5 K. b) Dispersion of the exciton bands (cf. Fig. 5b). c) Transient emission spectrum of a poly-crystalline PTCDA film at 5 K (time window $0 - 40\,\mathrm{ps}$ after short pulse excitation, streak-camera measurement, no correction for spectral instrument response).

VI. CONCLUSION

We presented a model Hamiltonian which includes several vibronic Frenkel and one nearest-neighbor CT exciton and is capable of describing energetic positions, peak intensities and polarization directions of a one-dimensional crystal. In crystals containing only one type of molecules, CT excitons are usually considered to have a very small intrinsic oscillator strength. Therefore, electro-absorption measurements are regarded as the most appropriate tool for their direct observation [8]. We demonstrate that in quasi-1D crystals with strong orbital overlap the CT excitons can have a considerable intrinsic transition dipole moment, which influences the polarization direction of the mixed exciton. In a three-dimensional crystal with two molecules per unit cell and weak coupling between the one-dimensional stacks, the CTE transition dipole affects the observable polarization ratio. This mechanism is discussed as a direct, qualitative proof for the mixing of Frenkel and CT excitons in MePTCDI independent of electro-absorption measurements.

Our model has been applied to polarized absorption spectra of the perylene derivative MePTCDI. Using a fitting procedure, a set of six model parameters Δ^0_{F}, Δ_{CT}, M, $|\epsilon_+|$, $p^{\mathrm{rel}}_{\mathrm{CT}}$, and F_0 was obtained to describe the 12 independent experimental values for the peak positions and intensities. The model fit can qualitatively explain all features of the absorption spectra. Because of the simplifications and the arbitrary weighting factors in the fit, the obtained parameters can not be considered as quantitative. However, we have shown that our model is capable of representing qualitatively the physical situation in the considered organic crystal. From a simplified analysis we find a similar picture for PTCDA. The order of magnitude of the proposed model parameters is confirmed by

a quantum chemical analysis.

As discussed in the introduction, the small radius exciton model applied here is only justified if the nearest-neighbor CT exciton is energetically well separated from higher energy CTE and especially from the free charge carrier bands. The binding energy of the lowest CTE in the stack is $\approx 1.9\,\mathrm{eV}$ and the next highest CTE lies already $\approx 0.7\,\mathrm{eV}$ higher [58]. This energetic separation is clearly larger than the charge transfer integrals included in $\epsilon_+(\mathrm{MePTCDI}) = 0.1\,\mathrm{eV}$, and the corresponding combined bandwidth for electrons and holes of $0.4\,\mathrm{eV}$ is also smaller than the binding energy of the lowest CTE. Therefore, the necessary conditions for a small radius exciton model which includes only the (electronically) lowest Frenkel and CT states are fulfilled.

Acknowledgements:

We wish to thank S. Hirschmann and N. Karl for performing the X-ray measurements and discussing their interpretation. We thank Z.G. Soos and P. Petelenz for stimulating discussions about excitons in organic crystals. M.H. acknowledges financial support by the Deutsche Forschungsgemeinschaft. V.M.A. thanks the Technische Universität Dresden for hospitality and support. He also acknowledges partial support through Grant 99-03-32178 of the Russian Foundation of Basic Research and Grant 97-1074 "Physics of Nanostructures" of the Russian Ministry of Science and Technology.

APPENDIX A: QUANTUM CHEMICAL CALCULATION OF CT TRANSITION DIPOLE MOMENTS

Here, we give a qualitative picture for the expected direction of the charge transfer transition dipole $\vec{p}_{\mathrm{CT}}$ and a schematic description of our quantum chemical calculations. Since we want to consider only nearest-neighbor CT states in the 1D-stacks, it is sufficient to know the properties of a dimer which has the same geometry as in the crystal. In order to give a conceptually simple picture, we discuss the quantum chemical description in terms of a semi-empirical Hartree-Fock calculation for the valence electrons and singly excited configurations (HF+CIS).

In an isolated MePTCDI-like molecule, the HOMO (H) is energetically well separated from lower lying molecular orbitals, and similarly, the LUMO (L) lies well below the next higher orbitals. Therefore, the lowest excited singlet state results from an almost pure HOMO-LUMO transition (compare [29] and our results below). Then, the excited states of the weakly interacting van-der-Waals dimer AB can be constructed out of (i) molecular excitations at A and B: $|\mathrm{ME_A}\rangle = |H_\mathrm{A} \rightarrow L_\mathrm{A}\rangle$ and $|\mathrm{ME_B}\rangle = |H_\mathrm{B} \rightarrow L_\mathrm{B}\rangle$, and (ii) CT excitations: $|\mathrm{CT_{A\rightarrow B}}\rangle = |H_\mathrm{A} \rightarrow L_\mathrm{B}\rangle$ and $|\mathrm{CT_{B\rightarrow A}}\rangle = |H_\mathrm{B} \rightarrow L_\mathrm{A}\rangle$. From this, a symmetry adapted basis set can be formed consisting of Frenkel excitons

$$|\mathrm{FE}_\pm\rangle = \frac{1}{\sqrt{2}}(\,|\mathrm{ME_A}\rangle \pm |\mathrm{ME_B}\rangle\,) \qquad \text{(A1)}$$

and delocalized CT excitons

$$|\mathrm{CT}_\pm\rangle = \frac{1}{\sqrt{2}}(\,|\mathrm{CT_{A\rightarrow B}}\rangle \pm |\mathrm{CT_{B\rightarrow A}}\rangle\,)\,. \qquad \text{(A2)}$$

The transition dipole moment $\vec{p}_{\mathrm{CT}} = \langle \mathrm{CT}_+|\hat{\vec{p}}|0\rangle$ of the symmetrical CT state is given by $\vec{p}_{\mathrm{CT}} = 2e\int \varrho_{\mathrm{AB}}\vec{r}\,dV$, where $\varrho_{\mathrm{AB}}(\vec{r}) = H_\mathrm{A}(\vec{r})L_\mathrm{B}(\vec{r})$ is the transition density between H_A and L_B.

Mulliken et al. described the behavior of such transition dipole matrix elements for a CT transition $|\mathrm{CT_{D\rightarrow A}}\rangle$ in donor-acceptor complexes ([59], p.28f and [60]). In this case, the transition density is typically discussed for a σ-type overlap, in which $\varrho_{\mathrm{DA}}(\vec{r})$ forms a small cloud without nodes and is localized between the two molecules. Then, the CT transition dipole can be visualized as the transfer of an electron from the donor D to the center between D and A. The direction of $\vec{p}_{\mathrm{CT}}$ is along the connection line. In our case of co-facially stacked aromatic molecules, ϱ_{AB} is formed by large and complicated π-orbitals. Although ϱ_{AB} is still located between the molecules, it is not concentrated in a small volume but forms a flat, quasi-two dimensional cloud with dimensions of the molecular size. Furthermore, like the contributing monomer orbitals, it now has a complicated node structure with alternating sign. Therefore, the transition dipole $\vec{p}_{\mathrm{CT}}$ cannot be estimated by simple geometrical considerations anymore. It is only clear that, very much in contrast to the Mulliken picture, $\vec{p}_{\mathrm{CT}}$ should lie approximately parallel to the molecular planes and not along the connection line. A strong transition dipole along this connection line is only caused by an asymmetry like in the donor-acceptor situation.

For actual calculations we used the semi-empirical ZINDO/S module of HyperChem 5.01 (Hypercube, Inc., Waterloo, Canada). We employed standard parameters and the weighting factors for the orbital overlap $F_\sigma = 1.267$ and $F_\pi = 0.585$ [61]. The atomic positions were taken from the geometry in the crystal structure (MePTCDI: [30], PTCDA: [13–16]). From the Hartree-Fock calculation of a monomer, the localized HF-orbitals $H_{\mathrm{A,B}}$ and $L_{\mathrm{A,B}}$ were obtained. For the calculation of the dimer, two approaches are generally possible: (i) Construction of dimer states from the monomer HF-orbitals as in (A1) and (A2) or (ii) HF+CIS calculation of the complete dimer and subsequent projection onto Frenkel and CT states (supermolecular approach). We used the second approach since a dimer calculation can be directly carried out by standard software. Our projection is similar to the analysis of phthalocyanine dimers in [62]. After calculating the dimer, we projected the two highest occupied dimer orbitals onto $H_\pm = 1/\sqrt{2}(H_\mathrm{A} \pm H_\mathrm{B})$ and the two lowest unoccupied dimer orbitals onto $L_\pm = 1/\sqrt{2}(L_\mathrm{A} \pm L_\mathrm{B})$. Using this projection, all results of CIS calculations (10 occupied and 12 unoccupied dimer orbitals) were expressed with the orbitals $H_\pm$ and $L_\pm$. The four lowest excited singlet states are mainly constructed from these $H_\pm$ and $L_\pm$ orbitals. That means, that the lowest states from a full dimer calculation can indeed be well described by the four Frenkel and CT configurations (A1) and (A2). The contribution of other configurations (sum of squared CI-coefficients) is less then 10% for MePTCDI or 17% for PTCDA.

Since only states of the same symmetry mix, there are two dipole allowed singlets $\mathrm{S}^{\mathrm{g}}_{1,2}$ and two dipole forbidden ones $\mathrm{S}^{\mathrm{u}}_{1,2}$ represented by linear combinations of either symmetrical

or antisymmetrical Frenkel and CT states:

$$|\mathrm{S}^{\mathrm{g}}_{1,2}\rangle = \alpha^{\mathrm{g}}_{1,2}|\mathrm{FE}_{+}\rangle + \beta^{\mathrm{g}}_{1,2}|\mathrm{CT}_{+}\rangle \qquad \text{(A3)}$$

$$|\mathrm{S}^{\mathrm{u}}_{1,2}\rangle = \alpha^{\mathrm{u}}_{1,2}|\mathrm{FE}_{-}\rangle + \beta^{\mathrm{u}}_{1,2}|\mathrm{CT}_{-}\rangle \qquad \text{(A4)}$$

From the coefficients in this representation, the desired transition dipoles $\vec{p}_{\mathrm{FE}} = \langle \mathrm{FE}_{+}|e\vec{r}|0\rangle$ and especially $\vec{p}_{\mathrm{CT}} = \langle \mathrm{CT}_{+}|e\vec{r}|0\rangle$ can finally be expressed through the directly calculated transition dipoles of the singlets $|\mathrm{S}^{\mathrm{g}}_{1,2}\rangle$.

The actual calculations confirm the qualitative expectations: $\vec{p}_{\mathrm{FE}}$ points along the long molecular axis and $\vec{p}_{\mathrm{CT}}$ makes a small angle with the molecular plane (MePTCDI: $20.4°$, PTCDA: $26.1°$). The CT transition dipole is much smaller but still considerable compared to the molecular transition dipole. The relative size $p^{\mathrm{rel}}_{\mathrm{CT}} := p_{\mathrm{CT}}/p_{\mathrm{ME}}$ is obtained as $p^{\mathrm{rel}}_{\mathrm{CT}} = 0.19$ for MePTCDI and $p^{\mathrm{rel}}_{\mathrm{CT}} = 0.14$ for PTCDA. The angle γ between the CT transition dipole component within the molecular plane and the long molecular axis is $\gamma = 68.1°$ for MePTCDI and $\gamma = 143.7°$ for PTCDA, i.e, in particular in MePTCDI the CT transition dipole has a large component along the molecular M-axis.

Furthermore, all electronic parameters used in the 1D-Hamiltonian (1) can be derived from the decomposition (A3) and (A4). The final results are for MePTCDI: $\Delta_{\mathrm{F}} = 2.89\,\mathrm{eV}$, $\Delta_{\mathrm{CT}} = 3.09\,\mathrm{eV}$, $M = 0.20\,\mathrm{eV}$, $|\epsilon_{+}| = 0.16\,\mathrm{eV}$, $|\epsilon_{-}| = 0.05\,\mathrm{eV}$; and for PTCDA: $\Delta_{\mathrm{F}} = 2.86\,\mathrm{eV}$, $\Delta_{\mathrm{CT}} = 3.05\,\mathrm{eV}$, $M = 0.19\,\mathrm{eV}$, $|\epsilon_{+}| = 0.05\,\mathrm{eV}$, $|\epsilon_{-}| = 0.04\,\mathrm{eV}$. These numerical values have to be considered as rough estimates just on the level of the used quantum chemical method. ZINDO/S and similar methods use atomic orbitals and semi-empirical parameters that are optimized for the conditions of bound atoms *within* a molecule. The situation *between* two unbound molecules may be very poorly characterized. For this reason, and also because any crystal environment is neglected, the determined interaction integrals M, $\epsilon_{\pm}$ and also the energy difference $\Delta_{\mathrm{CT}} - \Delta_{\mathrm{F}}$ may differ considerably from the values in the real crystal. In contrast, the geometric arrangement of the orbitals and thereby the direction of the transition moments should be only weakly sensitive to the level of approximation. The general trend of strong mixing between Frenkel and CT states agrees with quantum chemical studies on dimers with comparable π-electron overlap, e.g. on phthalocyanines [62] or polyenes [63].

[1] E.I. Rashba, M.D. Sturge (Eds.), Excitons, North-Holland, Amsterdam, 1982.
[2] V.M. Agranovich, A.A. Zakhidov, Chem. Phys. Lett. 50 (1977) 278.
[3] M. Pope, C.E. Swenberg, Electronic Processes in Organic Crystals, Oxford University Press, Oxford, 1999.
[4] D.S. Chemla, J. Zyss, Nonlinear Optical Properties of Organic Molecules and Crystals, Academic Press, Orlando, 1987.
[5] L. Sebastian, G. Weiser, H. B¨assler, Chem. Phys. 61 (1981) 125.
[6] L. Sebastian, G. Weiser, G. Peter, H. B¨assler, Chem. Phys. 75 (1983) 103.
[7] R.E. Merrifield, J. Chem. Phys. 34 (1961) 1835.
[8] P. Petelenz, M. Slawik, K. Yokoi, M.Z. Zgierski, J. Chem. Phys. 105 (1996) 4427.
[9] C.W. Tang, Appl. Phys. Lett. 48 (1986) 183.
[10] Z.D. Popovic, R.O. Loutfy, A.-M. Hor, Can. J. Chem. 63 (1985) 134.
[11] S.R. Forrest, Chem. Rev. 97 (1997) 1793.
[12] G. Klebe, F. Graser, E. H¨adicke, J. Berndt, Acta Cryst. B45 (1989) 69.
[13] A.J. Lovinger, S.R. Forrest, M.L. Kaplan, P.H. Schmidt, T. Venkatesan, J. Appl. Phys. 55 (1984) 476.
[14] A.J. Lovinger, S.R. Forrest, M.L. Kaplan, P.H. Schmidt, T. Venkatesan, Bull. Am. Phys. Soc. 28 (1983) 363.
[15] A.J. Lovinger, S.R. Forrest, M.L. Kaplan, P.H. Schmidt, T. Venkatesan, Bull. Am. Phys. Soc. 28 (1983) 476.
[16] M.L. Kaplan, C.S. Day, A.J. Lovinger, P.H. Schmidt, S.R. Forrest, full set of crystal structure data, private communication 1994.
[17] M.H. Hennessy, Z.G. Soos, R.A. Pascal Jr., A. Girlando, Chem. Phys. 245 (1999) 199.
[18] M. Hoffmann, K. Schmidt, T. Fritz, T. Hasche, V.M. Agranovich, K. Leo, in F. Kajzar, V.M. Agranovich (Eds.), Multiphoton and Light Driven Multielectron Processes: Materials, Phenomena, Applications, Kluwer, Dordrecht, 2000, p. 123.
[19] V. Bulović, P.E. Burrows, S.R. Forrest, J.A. Cronin, M.E. Thompson, Chem. Phys. 210 (1996) 1.
[20] E.I. Haskal, Z. Shen, P.E. Burrows, S.R. Forrest, Phys. Rev. B 51 (1995) 4449.
[21] K. Akers, R. Aroca, A.M. Hor, R.O. Loutfy, J. Phys. Chem. 91 (1987) 2954.
[22] K. Akers, R. Aroca, A.M. Hor, R.O. Loutfy, Spectrochim. Acta 44A (1988) 1129.
[23] K. Puech, H. Fr¨ob, M. Hoffmann, K. Leo, Optics Lett. 21 (1996) 1606.
[24] U. Gómez, M. Leonhardt, H. Port, H.C. Wolf, Chem. Phys. Lett. 268 (1997) 1.
[25] K. Puech, H. Fr¨ob, K. Leo, J. Lum. 72-74 (1997) 524.
[26] P.B. Bisht, K. Fukuda, S. Hirayama, J. Phys. Chem. B 101 (1997) 8054.
[27] V. Bulović, S.R. Forrest, Chem. Phys. 210 (1996) 13.
[28] C.I. Wu, Y. Hirose, H. Sirringhaus, A. Kahn, Chem. Phys. Lett. 272 (1997) 43.
[29] M. Adachi, Y. Murata, S. Nakamura, J. Phys. Chem. 99 (1995) 14240.
[30] E. H¨adicke, F. Graser, Acta Cryst. C42 (1986) 189.
[31] P.M. Kazmaier, R. Hoffmann, J. Am. Chem. Soc. 116 (1994) 9684.
[32] F.F. So, S.R. Forrest, Y.Q. Shi, W.H. Steier, Appl. Phys. Lett. 56 (1990) 674.
[33] F.F. So, S.R. Forrest, Phys. Rev. Lett. 66 (1991) 2649.
[34] D.P. Craig, J. Chem. Soc. (1955) 2302.
[35] D.P. Craig, S.H. Walmsley, Excitons in Molecular Crystals. Theory and Applications, Benjamin, New York 1968.
[36] V.M. Agranovich, Sov. Phys. Sol. State 3 (1961) 592.
[37] V.M. Agranovich, Fiz. Tverd. Tela 3 (1961) 811.
[38] A.S. Davydov, Theory of molecular excitons, Plenum Press, New York 1971.
[39] V.M. Agranovich, M.D. Galanin, Electronic Excitation Energy Transfer in Condensed Matter, North-Holland Publishing Com-

pany, Amsterdam 1982.
[40] M.H. Hennessy, Z.G. Soos, V. Bulović, S.R. Forrest, Mat. Res. Symp. Proc. Vol. 488 (1998) 171.
[41] M.H. Hennessy, R.A. Pascal Jr., Z.G. Soos, Proc. SPIE 3797 (1999) 89.
[42] R. Scholz, Y.Yu. Kobitski, T.U. Kampen, M. Schreiber, D.R.T. Zahn, G. Jungnickel, M. Elstner, M. Sternberg, Th. Frauenheim, Phys. Rev. B 61 (2000), *in press*.
[43] H. Suzuki, Electronic Absorption Spectra and Geometry of Organic Molecules, Academic Press, New York 1967.
[44] U.-M. Gómez, Abstandsabh¨angiger Energietransfer ultrad¨unner MePTCDI-Schichten zum dielektrischen Substrat, PhD thesis, Stuttgart, 1997 (Shaker Verlag Aachen, 1997).
[45] D.B. Fitchen, Zero-phonon transitions, in: W.B. Fowler (Ed.), Physics of color centers, Academic Press New York, 1968.
[46] F. Graser, E. H¨adicke, Liebigs Ann. Chem. 1984, 483.
[47] K. Keller (Ed.), Science and Technology of Photography, VCH Weinheim, 1993.
[48] V.M. Agranovich, V.L. Ginzburg, Crystal Optics with Spatial Dispersion and Excitons, Springer, Berlin 1984.
[49] A.B. Djurišić, T. Fritz, K. Leo, Optics Comm. 166 (1999) 35.
[50] N. Karl, J. Marktanner, Mol. Cryst. Liq. Cryst. 315 (1998) 163.
[51] H. Yanagi, Y. Toda, T. Noguchi, Jpn. J. Appl. Phys. 34 (1995) 3808.
[52] M. M¨obus, N. Karl, T. Kobayashi, J. Cryst. Growth, 116 (1992) 495.
[53] D.Y. Zang, F.F. So, S.R. Forrest, Appl. Phys. Lett. 59 (1991) 823.
[54] Z.G. Soos, M.H. Hennessy, G. Wen, Chem. Phys. 227 (1998) 19.
[55] M. Andrzejak, G. Mazur, P. Petelenz, J. Mol. Struc./THEOCHEM, *in press*.
[56] H.C. Wolf, Advances in atomic and molecular physics, Vol. 3, New York 1697, p. 119.
[57] M. Born, K. Huang, Dynamical Theory of Crystal Lattices, Oxford University Press, Oxford 1954.
[58] Z. Shen, S.R. Forrest, Phys. Rev. B. 55 (1997) 10578.
[59] R.S. Mulliken, W.B. Person, Molecular Complexes. A Lecture and Reprint Volume, Wiley-Interscience, New York 1969.
[60] R.S. Mulliken, J. Am. Chem. Soc. 64 (1952) 811.
[61] A.D. Bacon, M.C. Zerner, Theoret. Chim. Acta, 53 (1979) 21.
[62] N. Ishikawa, O. Ohno, Y. Kaizu, H. Kobayashi, J. Phys. Chem. 96 (1992) 8832.
[63] D. Beljonne, J. Cornil, R. Silbey, P. Millé, J.L. Brédas, J. Chem. Phys. 112 (2000) 4749.